Surv. Geophys manuscript No.
(will be inserted by the editor)

Synergies of Spaceborne Imaging Spectroscopy with other Remote Sensing Approaches

Luis Guanter[1], Maximilian Brell[1], Jonathan C.-W. Chan[2], Claudia Giardino[3], Jose Gomez-Dans[4], Christian Mielke[1], Felix Morsdorf[5], Karl Segl[1], Naoto Yokoya[6]

[1]Helmholtz Centre Potsdam German Centre for Geosciences (GFZ), Potsdam, Germany
[2]Department of Electronics and Informatics, Vrije Universiteit Brussel, Brussels, Belgium
[3]CNR-IREA, Institute for Electromagnetic Sensing of the Environment, Milan, Italy
[4]Department of Geography and National Centre for Earth Observation, University College London, UK
[5]Remote Sensing Laboratories, Department of Geography, University of Zurich, Switzerland
[6]RIKEN Center for Advanced Intelligence Project, Tokyo, Japan

Abstract Imaging spectroscopy (IS), also commonly known as hyperspectral remote sensing, is a powerful remote sensing technique for the monitoring of the Earth's surface and atmosphere. Pixels in optical hyperspectral images consist of continuous reflectance spectra formed by hundreds of narrow spectral channels, allowing an accurate representation of the surface composition through spectroscopic techniques. However, technical constraints in the definition of imaging spectrometers make spectral coverage and resolution to be usually traded by spatial resolution and swath width, as opposed to optical multispectral (MS) systems typically designed to maximize spatial and/or temporal resolution. This complementarity suggests that a synergistic exploitation of spaceborne IS and MS data would be an optimal way to fulfill those remote sensing applications requiring not only high spatial and temporal resolution data, but also rich spectral information. On the other hand, IS has been shown to yield a strong synergistic potential with non-optical remote sensing methods, such as thermal infrared (TIR) and light detection and ranging (LiDAR). In this contribution we review theoretical and methodological aspects of potential synergies between optical IS and other remote sensing techniques. The focus is put on the evaluation of synergies between spaceborne optical IS and MS systems because of the expected availability of the two types of data in the next years. Short reviews of potential synergies of IS with TIR and LiDAR measurements are also provided.

Keywords Imaging spectroscopy · multispectral remote sensing · synergy · data fusion · spatial enhancement · thermal infrared · LiDAR

1 Introduction

Imaging spectroscopy (IS) in the optical domain, also known as hyperspectral remote sensing, is an Earth observation technique based on spectrally-contiguous measurements of the solar light reflected by the

L. Guanter
Helmholtz Centre Potsdam German Centre for Geosciences (GFZ)
Telegrafenberg A17 14473 Potsdam, Germany
Tel.:+49-3312881190
Fax: +49-3312881192
E-mail: guanter@gfz-potsdam.de

Earth's surface and atmosphere (Goetz et al., 1985). Each pixel in the resulting hyperspectral images contains a continuous spectrum sampling absorption features which can be linked to the pixel composition. Due to this generic measurement principle, IS provides an accurate representation of geobiophysical parameters, which can be used to infer quantitative information on a wide range of Earth's surface parameters and processes.

The raise and consolidation of IS as a powerful remote sensing technique for land monitoring over the last three decades has mostly relied on airborne spectrometers. In particular, the NASA Jet Propulsion Laboratory's Airborne Visible/Infrared Imaging Spectrometer (AVIRIS) (Green et al., 1998), covering the 400–2500 nm spectral range (visible to shortwave infrared, VSWIR) with 10-nm wide spectral channels, has been used in a large number of campaigns across different continents and ecosystems (e.g. Thompson et al., 2017). From a satellite perspective, the Hyperion spectrometer onboard NASA's Earth Observing One (EO-1) spacecraft was a technology demonstration project which operated between 2001 and 2017 (Ungar et al., 2003). Hyperion acquired hyperspectral images with a 30 m ground sampling distance (GSD), a 7 km horizontal swath and a spectral coverage and sampling similar to that of AVIRIS, although with a much lower radiometric performance and overall data quality. Other satellite IS projects, in this case restricted to the visible near-infrared (VNIR, 400–1000 nm) spectral region, are the Compact High Resolution Imaging Spectrometer (CHRIS) on ESA's Proba-1 microsatellite (Barnsley et al., 2004), which has been operating since 2001, and the Hyperspectral Imager for the Coastal Ocean (HICO) (Lucke et al., 2011), developed by NASA and the US Office of Naval Research and operating onboard the International Space Station (ISS) between 2009 and 2015.

After those technology demonstration projects, several scientific missions expected to deliver accurate spectroscopic measurements are scheduled for the next years. In particular, the Environmental Mapping and Analysis Program (EnMAP) is a German mission which will measure in the VSWIR spectral range with an average spectral sampling of 10 nm, a 30 m GSD, a 30 km swath width and a revisit time under quasi-nadir observation of less than 4 weeks (Guanter et al., 2015). These characteristics are shared by the Italian Space Agency's PRISMA (Hyperspectral Precursor of the Application Mission) (Candela et al., 2016), which in addition presents a panchromatic channel with a 5 m GSD. Other projects, such as NASA's Hyperspectral Infrared Imager (HyspIRI) (Lee et al., 2015), and the Italian-Israeli SHALOM (Spaceborne Hyperspectral Applicative Land and Ocean Mission), currently awaiting the final decision for implementation, could follow EnMAP and PRISMA by mid 2020s.

In general, upcoming space-based VSWIR IS missions such as EnMAP and PRISMA are expected to provide hyperspectral data in a higher data-rate and radiometric and spectral quality than their predecessor Hyperion. However, due to trade-offs in spectrometer design between spatial resolution, spectral resolution, swath width, and signal-to-noise ratio (SNR), spaceborne IS missions are usually designed to acquire data with a moderate GSD (typically 30 m) as well as with a small across-track swath, which results in a nadir revisit time of up to 4 weeks. It must also be mentioned that EnMAP and PRISMA are "site-oriented" missions, which means that they are tasked on a daily basis to acquire images over selected sites, as opposed to "wall-to-wall" mapping missions with systematic full global coverage. Temporal resolution will be improved by EnMAP and PRISMA through across-track pointing, but this can only happen over a limited number of sites per day due to the high impact of platform pointing maneuvers on mission operations. Those sampling limitations will hamper the use of EnMAP, PRISMA and similar missions for those applications requiring high temporal resolution (e.g. those dealing with water and vegetation) or spatial resolution (e.g. land cover mapping or mineral exploration).

The EnMAP and PRISMA spaceborne IS missions are expected to co-exist with a number of other satellite missions based on different measurement principles, and especially with optical multispectral (MS) missions. An overview of some operating and upcoming satellite missions mentioned in this paper is provided in Table 1. For example, the ESA/Copernicus Sentinel-2 mission (Drusch et al., 2012), which has an optical multispectral imager (MSI) as main payload, is planned for long-term operations and will coexist with EnMAP, PRISMA and other future IS missions. Sentinel-2 MSI has a wide spatial coverage (290 km

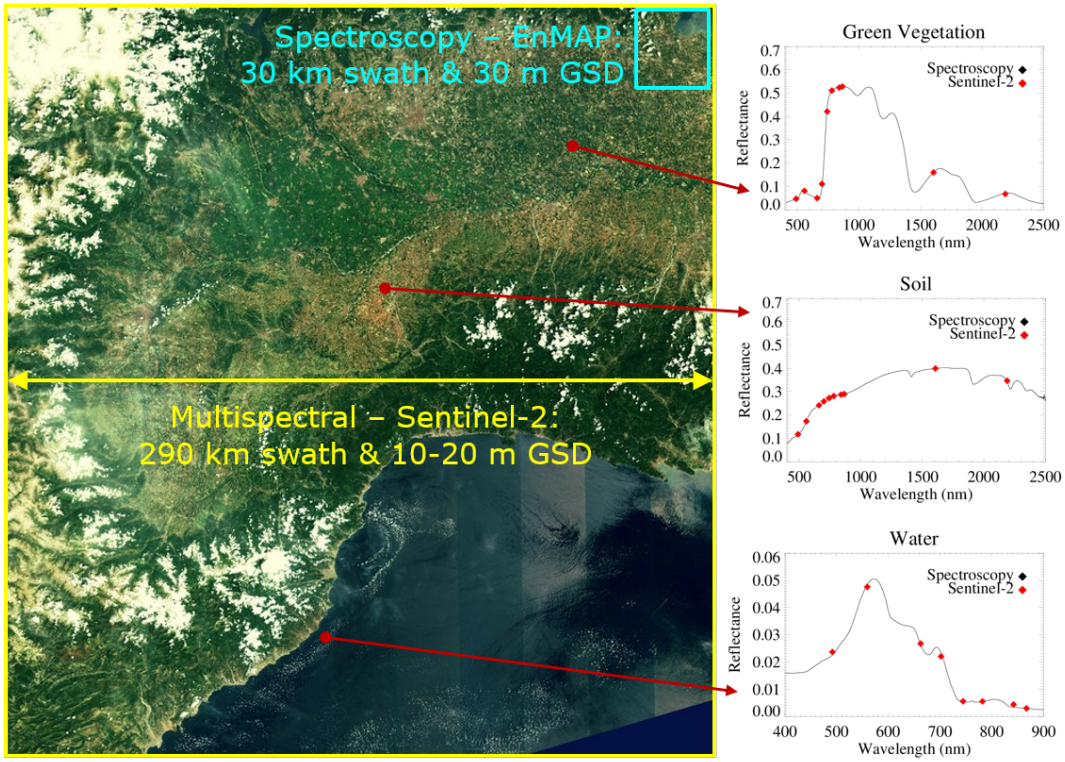

Fig. 1 First image from Sentinel-2A covering parts of Italy and France in June 2015. The spatial coverage of Sentinel-2 is compared to that of the EnMAP imaging spectroscopy mission. Panels on the right hand side compare surface reflectance spectra as acquired by an imaging spectrometer and the 10–20 m channels in the multispectral imager (MSI) on Sentinel-2. GSD stands for ground sampling distance.

swath), VSWIR spectral coverage (13 spectral channels between 440 and 2200 nm), high spatial resolution (10 spectral channels at 10 or 20 m ground sampling distance), high temporal resolution (5-day revisit time) and open data policy. Also Landsat-8/9 missions (Roy et al., 2014) offer spatially continuous VSWIR MS data and will co-exist with EnMAP and PRISMA. Optical MS missions such as Sentinel-2 and Landsat hold a strong potential for synergistic use with EnMAP-like IS missions, since the poorer spectral information of the multispectral data is compensated by their improved spatial coverage, temporal resolution, and (in the case of Sentinel-2) spatial resolution. This is illustrated in Fig. 1. The combination of optical IS and MS missions can thus be used for a temporal and/or spatial enhancement of the rich spectral information provided by the IS data set. This is also the rationale for the inclusion of a panchromatic channel in the PRISMA mission concept (Candela et al., 2016) and for the joint deployment of Hyperion and the Advanced Land Imager (ALI) onboard the EO-1 platform.

A different type of synergy with IS data would be the one consisting in the combination of IS measurements with those derived from non-optical instruments carrying fundamentally different information. This would be, for instance, the combination of IS and light detection and ranging (LiDAR) data, which can be very useful for e.g. the classification of urban objects or the chracterization of vegetation covers. The latter is main purpose of the Carnegie Airborne Observatory intended for ecological research, which combines airborne spectroscopy and a dual-laser waveform LiDAR scanner (Asner et al., 2012). Regarding other spectral ranges, the HyspIRI mission concept relies on the combination of spaceborne hyperspectral

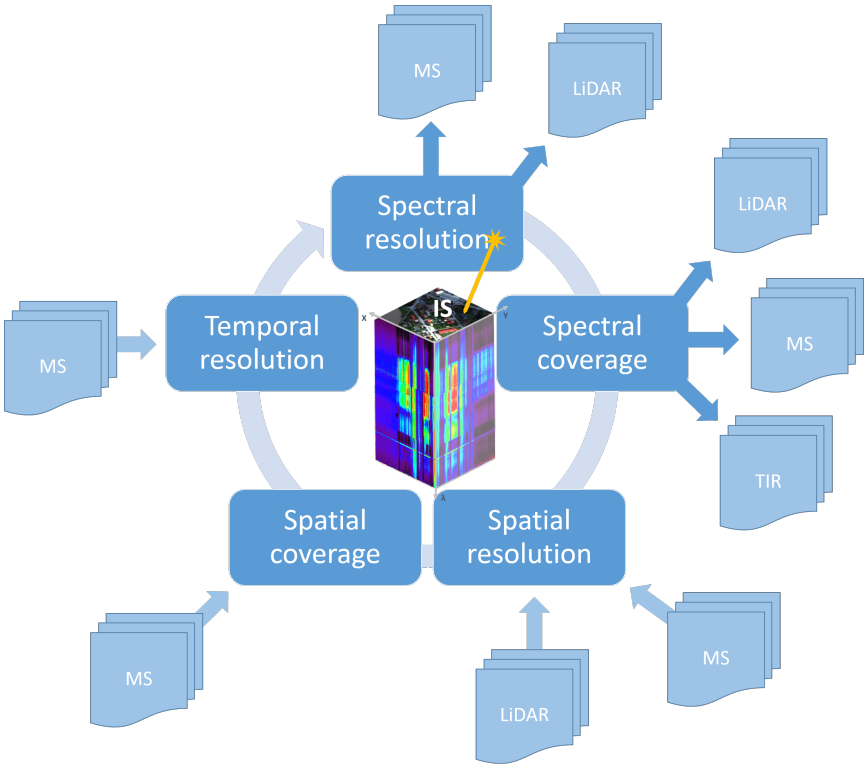

Fig. 2 Schematic view of how synergies between imaging spectroscopy and other remote sensing techniques can be used to improve spectral, spatial and temporal sampling in the resulting data set. IS stands for imaging spectroscopy, MS for optical multispectral data and TIR for thermal infrared.

VSWIR and thermal infrared (TIR) measurements in order to address a number of scientific questions related to the Earth's ecosystems (Lee et al., 2015). Synergies between IS and TIR measurements are also considered for the ESA FLuorescence EXplorer (FLEX) mission (Drusch et al., 2017). FLEX will provide spectroscopic measurements in the 500–800 nm spectral window at high spectral resolution (<3 nm) and low spatial resolution (GSD=300 m) for the retrieval of chlorophyll fluorescence and other plant biochemical parameters. FLEX will fly in tandem with the Sentinel-3 mission adding TIR measurements necessary for the interpretation of the fluorescence measurements from FLEX. On the other hand, an exceptional wealth of information for ecosystem research will become available from the combined operation of a series of remote sensing instruments to be deployed at the ISS in 2018. This will include the Global Ecosystem Dynamics Investigation (GEDI) LiDAR, the Ecosystem Spaceborne Thermal Radiometer Experiment on Space Station (ECOSTRESS), and the Orbiting Carbon Observatory 3 (OCO-3), all three from NASA, and the VSWIR Hysperspectral Imager Suite (HISUI) from the Japanese Ministry of Economy, Trade, and Industry (METI). The combination of those four instruments will provide key information on canopy structure (GEDI), evapotranspiration and stress (ECOSTRESS), chlorophyll fluorescence (OCO-3) and ecosystem composition and plant traits (HISUI), which will be used to investigate vegetation functioning at the ecosystem scale during the time period in which the 4 instruments will be operated (Stavros et al., 2017).

This contribution reviews potential synergies between IS data and other remote sensing techniques. The focus is on the discussion of theoretical aspects and methodological issues, rather than on a comprehensive

Table 1 Observation parameters of some of the satellite missions mentioned in this paper. IS stands for imaging spectrometer, MS for multispectral instrument, VSWIR for visible to shortwave infrared, VNIR for visible near-infrared, SWIR for shortwave infrared, TIR for thermal infrared, GSD for ground sampling distance, PAN for panchromatic channel, and ALI for advance land imager.

	Spectral sampling	**Spectral coverage**	**GSD (optical)**	**Revisit time**	**Status**	**Note**
EnMAP	IS	VSWIR	30 m	27 d nadir, ∼4 d with 30° pointing	Launch ∼2020	Acquisitions on request
PRISMA	IS	VSWIR	30 m	29 d nadir, ∼7 d with 15° pointing	Launch ∼2018	Acquisitions on request; 5 m PAN
HyspIRI	IS	VSWIR & TIR	30 m	5–16 d	Under evaluation	Global mapper with 185 km swath
Hyperion	IS	VSWIR	30 m	∼6 d with 22° pointing	End in 2017	Flight with MS ALI
CHRIS-Proba	IS	VNIR	17–34 m	∼6 d with 30° pointing	Operating	Multiangular capabilities
Landsat	MS	VSWIR & TIR	30 m	16 d	Operating	Long data record
Sentinel-2	MS	VSWIR	10–20 m	5 d	Operating	High spatio-temporal resolution
Sentinel-3	MS	VNIR & TIR	300 m	1 d	Operating	Focus on ocean monitoring
ASTER	MS	VSWIR & TIR	15–30 m	16 d	Operating	Good SWIR sampling (until 2008)

review of single examples in the literature. Special attention is put on the assessment of synergies between spacebased IS and optical MS missions because of the open and large scale data availability expected for the next years, thanks in particular to the co-existance of EnMAP, PRISMA, Sentinel-2 and Landsat missions. Theoretical considerations and some examples of those synergies between IS and optical MS missions are presented in Section 2. Potential synergies of IS with TIR and LiDAR measurements will be discussed in Section 3. A summary of key points and a discussion of the implications of synergistic approaches for the design and exploitation of future IS missions will be finally provided in Section 4.

2 Synergies of imaging spectroscopy with optical MS data

2.1 Approaches for synergistic use of optical IS and MS data

Synergies between spaceborne IS and optical MS measurements, e.g. from EnMAP/PRISMA and Sentinel-2, respectively, could be developed in at least two different directions:

- Enhancement of the spatial resolution of the IS data through fusion with higher resolution MS data
- Improvement of mapping capabilities through the joint exploitation of MS and IS data sets

The fundamental basis for these two types of synergistic approaches and some examples are discussed hereinafter in this section.

2.1.1 Enhancement of spatial resolution of IS data through fusion with MS data

Recently, considerable attention has been paid to the development of resolution enhancement techniques for IS imagery via IS and MS data fusion (Yokoya et al., 2017). The resolution enhancement of IS imagery can be performed by fusing a low-resolution IS image with a higher-resolution MS image, where both images are acquired over the same Earth's surface in the same season under similar atmospheric and illumination conditions. The resolution-enhanced IS data have the high spatial resolution of the MS sensor and the high spectral resolution of the IS sensor. Such high-order image products, which can be generated by using operational satellites (e.g., EnMAP and Sentinel-2), have the potential to enable a variety of new IS applications on a global scale, including high-resolution mapping of minerals, urban surface materials, and plant species.

The final goal for the sharpening of IS data would be the accurate reconstruction at high spatial resolution of not only the broadband spectral shape, but also the single absorption features present in the spectrum. From a theoretical point of view, an absorption feature in the IS data can only be spatially-sharpened with higher resolution MS data if (and only if) the IS spectra represent pure spectra at the MS resolution, and at least one of the following conditions holds:

1. the absorption feature is wide enough to be sampled by the MS instrument (e.g. chlorophyll or iron, see Fig. 3a)
2. the material causing the absorption feature of interest also presents absorption features in other parts of the spectrum which are wide enough to be sampled by the MS instrument (e.g. liquid water presents absorption features with varying depth within the entire 950–2500 nm window, see Fig. 3b)
3. the material causing the absorption feature of interest tends to co-exist with other materials presenting absorption features in parts of the spectrum sampled by the MS instrument (e.g. chlorophyll and liquid water contents tend to covary in healthy vegetation)

The increase of information content of the spatially-enhanced IS data would depend on which of those three conditions applies. In the case of (1), the absorption feature is already sampled at high spatial resolution in the MS data, but the spatially-enhanced IS data set would allow the application of band fitting retrieval algorithms, which can lead to more robust retrievals. Concerning (2), weaker absorption features can be spatially-enhanced through leverage with other parts of the spectrum at which the same material presents absorption features, the advantage of this being that the sharpened narrow features may be less affected by confounding factors than the wider ones sampled by the MS spectrum. As for (3), the spatial enhancement of absorption features would only map the statistical coexistence of different materials represented in the spectrum, and the resulting sharpened features would not represent actual changes in the surface composition or condition for those pixels in which the co-existence between the two materials deviates from the expectation.

To solve the IS and MS data fusion problem, researchers have proposed various methods in the last decade. The existing literature can be categorized into two groups. The first group of methods is based on pan-sharpening. Pan-sharpening is a technique that fuses low-resolution MS and higher-resolution panchromatic images to create a high-resolution MS image. Since pan-sharpening can be regarded as a special case of IS and MS data fusion, significant effort has been devoted to extending and generalizing existing pan-sharpening techniques for IS and MS data fusion. Representative methods include component substitution (Chen et al., 2014), multiresolution analysis (Selva et al., 2015), and patch-wise sparse representation methods (Grohnfeldt et al., 2013).

The second group of methods solves the problem through the analysis of the latent spectral characteristics of the observed scene based on a subspace spanned by a set of basis vectors or spectral signatures of underlying materials (so-called endmembers). This approach includes various methods based on matrix factorization (Yokoya et al., 2012), spectral unmixing (Lanaras et al., 2015), and Bayesian probability (Wei et al., 2015). For instance, unmixing-based methods reconstruct a high-resolution IS image by estimating

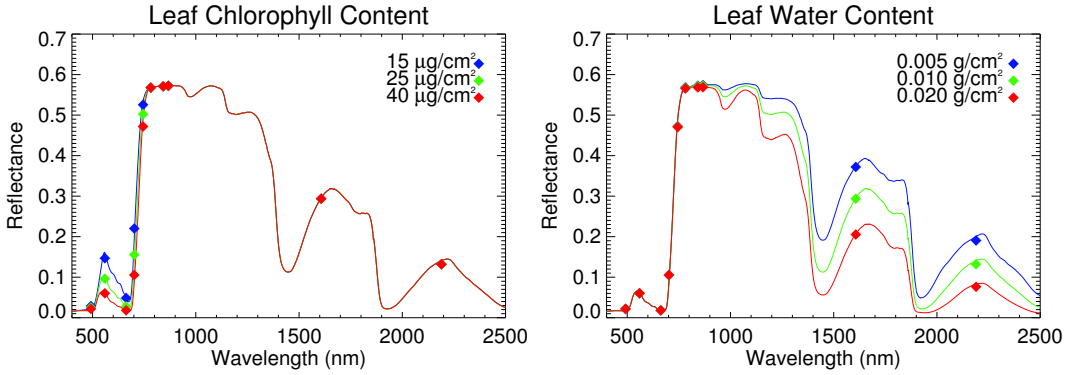

(a) (b)

Fig. 3 Top-of-canopy reflectance spectra at full spectral resolution and resampled to the 10–20 m channels of Sentinel-2 MSI for (a) different values of leaf chlorophyll content, and (b) different values of leaf water content.

spectral signatures of endmembers and high-resolution fractional abundances from the input IS and MS images, respectively.

Methods above have been recently compared with extensive experiments in a review paper by Yokoya et al. (2017). Multiresolution analysis based methods and unmixing based methods demonstrated good and stable performance with different fusion scenarios. Current research on the development of algorithms for IS and MS data fusion is focused on combining different approaches to further improve the reconstruction performance.

Fig. 4 presents an example of IS and MS data fusion using simulated EnMAP and Sentinel-2 images over an urban area of Brussels, Belgium. The fusion procedure is composed of two steps: 1) self-sharpening of Sentinel-2 data that sharpens the 20-m-GSD bands by the 10-m-GSD bands, and 2) the fusion of EnMAP and 10-m-GSD Sentinel-2 data. The multiresolution analysis based fusion technique presented in Selva et al. (2015) was used for both steps. As shown in the color composite images in Fig. 4, the spatial information content is significantly improved. On the other hand, the spectral profiles in Fig. 4 indicate that the spectral quality is variable particularly in the SWIR range where the spectral coverage of Sentinel-2 is limited with only two bands. The importance of the overlap of spectral response functions between two sensors is discussed in Yokoya et al. (2017).

Some publications have appeared in recent years reporting the impact of resolution enhancement of IS imagery on spectral unmixing (Yokoya et al., 2016) and land-cover classification (Chan and Yokoya, 2016). Due to inevitable spectral distortions in the resolution-enhanced data, the use of external spectral libraries does not always work for classification or spectral unmixing. In contrast, it has been shown that good results can be obtained in classification or spectral unmixing by using reference spectra acquired from each fused image (Yokoya et al., 2017, 2016).

Research on quality assessment of resolution-enhanced products is also important from a practical viewpoint; however, very few publications can be found compared to those dealing with algorithm development. Quantitative evaluation of resolution-enhanced data is usually performed within simulation studies because reference data are necessary to quantify reconstruction performance. When resolution-enhanced IS image products are generated from operational satellites (e.g., EnMAP and Sentinel-2), quantitative quality assessment without reference is required to provide spectral quality at each pixel so that users can identify and select reliable pixel spectra. The standard technique for this purpose is to examine consistency between the input images and degraded versions of the fused image using quality measures (Palsson et al., 2016).

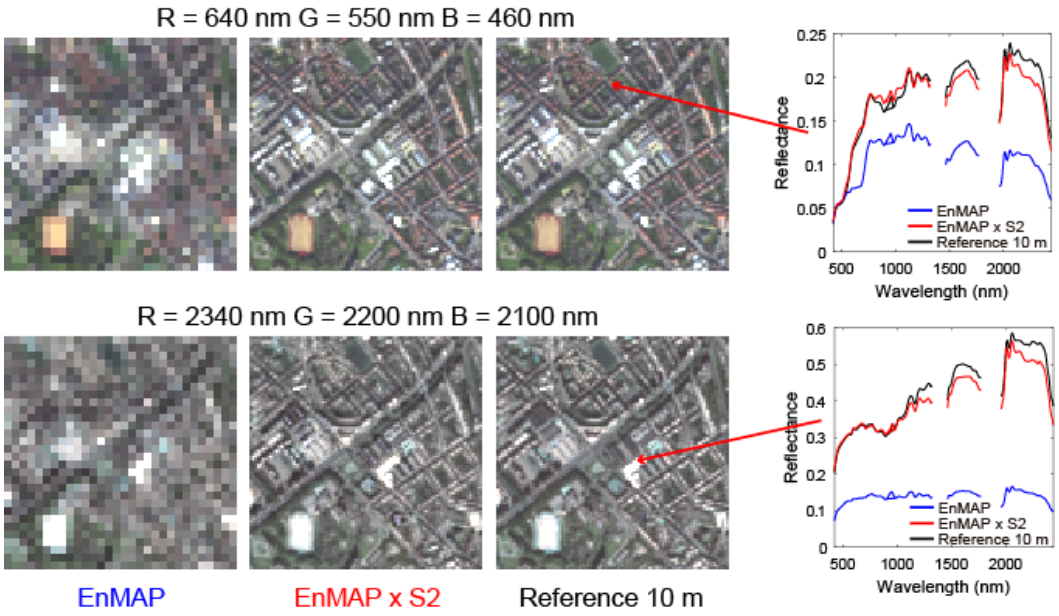

Fig. 4 Example of spatial enhancement of IS data. Color composite images of simulated EnMAP, EnMAP-Sentinel-2 fused, and reference data over an urban area of Brussels (Belgium) are shown together with spectral signatures for two locations.

There is still room for investigation on how to integrate the consistency information obtained for each of the two input images.

2.1.2 Improvement of mapping capabilities through the joint exploitation of MS and IS data sets

The high spectral resolution and coverage of IS instruments can also be used improved spatio-temporal monitoring with MS data. This could be achieved through, at least, (i) analysis of IS results for the interpretation of co-located MS measurements, and (ii) the extrapolation of IS-based information to the broad spatial and temporal coverage of the MS data set.

Analysis of IS results for the interpretation of MS measurements: the richer spectral information in the IS data complements the wider-area and higher spatio-temporal mapping capabilities of the MS instrument. For example, Milewski et al. (2017) combined EO-1 Hyperion data with multitemporal and multispectral Landsat acquisitions in order to analyze the spatial distribution of surface evaporite minerals and changes in a Namibian Kalahari salt pan, which is a semi-arid depositional environment associated with episodic flooding events. The dynamic of the surface crusts was evaluated through change detection analysis based on a time series of Landsat acquisitions (1984–2015), whereas a hyperspectral image from Hyperion was used to map the spatial distribution of the major crust types (halite, gypsum, calcite/sepiolite and disturbed, dark crust) and their abundances through spectral mixture analysis (SMA). The combined information from the hyperspectral and multispectral data sets could then be exploited to spatially differentiate and map depositional environments over the whole salt pan.

In a different study, Mielke et al. (2014a) assessed the potential of combined IS and MS spaceborne data for mapping the spatial extent of mine waste surfaces in South Africa. For that task, the broadband iron feature depth (IFD) index was proposed as a potential proxy for mine waste. The IFD derived from Landsat was found to be in good agreement with primary and secondary iron-bearing minerals mapped

from Hyperion data, which suggests that a combination of IS data for mineral identification with MS data for repetitive area-wide mapping of the IFD as a mine waste proxy is a promising synergistic application of IS and MS data. The use of the IFD index for geological applications based on combined IS and MS data will be further discussed in section 2.2.2.

Also dealing with geological mapping, Bishop et al. (2011) employed a two-step progressive approach, first to locate target areas characterized by hydrothermal mineral alteration using Advanced Spaceborne Thermal Emission and Reflection Radiometer (ASTER) VNIR and SWIR data, and secondly, to attempt detailed mineral mapping using Hyperion's spectral information.

Extrapolation of IS-based information to the broad spatial and temporal coverage of the MS data: In a different type of synergetic use of IS and MS data, the richer spectroscopic information delivered by the imaging spectrometer over a given area can be used to enhance the mapping potential of MS observations over a wider area than the one sampled by the IS data set.

For instance, Hubbard et al. (2003) combined Hyperion, EO–1 Advance Land Imager (ALI) and the co-orbiting ASTER data to map hydrothermally altered rocks associated with volcanic systems over the Central Andes. The mineral maps derived from Hyperion data with the Tetracorder expert system (Clark et al., 2003) were used to adjust image display thresholds in the alteration mineral maps derived from ALI and ASTER over a much broader area than the Hyperion coverage alone. Hyperion data were also used for the interpretation of ASTER and ALI mapping results as well as for their radiometric and atmospheric correction. A similar set-up was used by Hubbard and Crowley (2005) for mineral mapping over the Chilean–Bolivian Altiplano.

Schmid et al. (2005) used IS data to support the mapping of geophysical parameters in space and time with Landsat data. In particular, they developed an approach to monitor changes in wetlands in Central Spain. For this purpose, an SMA approach was used with a temporal series of Landsat data to detect changes in the wetland over time. The spectral endmembers for the SMA were extracted from hyperspectral data acquired during an airborne campaign, resampled to Landsat's TM and ETM+ spectral responses. It was used for change analysis at different and temporal scales, showing the feasibility of exploiting spectral endmembers derived from hyperspectral information in the analysis of MS data.

Concerning vegetation, optical MS measurements of vegetation reflectance spectra are generally sensitive to canopy water content (CWC), but quantitative estimates of CWC can only be reliably derived from IS radiance data through physical modeling of vapor and liquid water spectral features in the near-infrared. Asner et al. (2016) extrapolated CWC maps derived from airborne IS data over some sites to the entire state of California by means of a deep learning technique establishing empirical relationships between IS-based CWC and a series of parameters retrieved from Landsat and other ancillary data sets. The resulting California-wide CWC maps were analysed to assess the forest canopy water loss during the 2012–2015 California drought.

Model inversion and assimilation of multi-temporal data sets: Strategies for the combination of IS and MS data can be based on a physical modeling of the geophysical parameters to be inferred from the remote sensing data, which complements the empirical approaches discussed in sections 2.1.1 and 2.1.2. Broadly speaking, this physical modeling means that the scene (e.g. land surface vegetation, atmosphere, ...) can be parameterized by a finite set of metrics (e.g. leaf area index, leaf pigment concentrations, soil optical properties, ...). These parameters can all be combined in a so-called *state vector*. Each observation, be it IS or MS, would provide an *inference* of the scene parameters: an uncertainty-quantified estimate of the state vector, or more precisely, the probability density function of the state vector. Parameters that can be inferred well because a particular observation has a strong sensitivity to it will be characterised by low uncertainty, whereas parameters with a large uncertainty will be symptomatic of low sensitivity in the observations. The mapping from observation to state vector is accomplished by inverting the observations

using an *observation operator*, typically a physical model based on radiative transfer theory that produces a prediction of the sensor observations as a function of the state vector.

In the case of multi-temporal data sets consisting of both MS and IS acquisitions, dynamic physically-based models allow us to blend in observations from the two sensors in a physically consistent manner. In its simplest form, we can imagine a scenario where MS and IS sensors fly over the same scene simultaneously. We can then invert the observations from one sensor, and use the inferred state vector probability density function as the *a priori* distribution of the second observation, which will result in a physically-based combination of both, respecting the characteristics of both sensors. The use of an observation operator allows one to account for different sensor characteristics (different illumination/viewing geometries, spectral sampling, spatial resolution, ...). The retrieval system is in this case combining two independent inferences of the same scene, acquired at the same time, to come to a solution that is consistent with both. An example will be discussed in Section 2.2.3.

If observations do not happen simultaneously, a first approach might be to assume that within a temporal window, the scene changes little, and thus they can be assumed simultaneous. However, this assumption can be broken in a few days for the land surface, and in less than an hour for atmospheric parameters. Dynamic models might be used to propagate the state vector at one location from one time step to another. The simplest possible dynamic model is to assume that nothing is changing, but to use this model under the assumption that it is wrong, and thus as model propagates the state over longer and longer time gaps will add uncertainty to the original estimate. This uncertainty inflation approach is the basis of temporal regularization e.g. (Lewis et al., 2012). More sophisticated approaches will use a dynamic model that describes the evolution of the state vector, but the concept of model uncertainty is still important, as even in the hypothetical case that the model was perfect, changes in the scene would render it wrong.

The approach described above has been widely used for dynamical systems, as well as climate studies, where it often is referred to as ”data assimilation”. A number of standard techniques, such as Kalman and particle filters, variational approaches, have been exploited to this end with Earth observation data. The same approaches can be used for IS and MS data combinations, provided that a reasonable observation operator is used. An example is shown in Fig 5, where we show the EO-LDAS system introduced in Lewis et al. (2012) being used to invert observations of surface directional reflectance from MS sensors, Landsat 8 and Sentinel-2. In this experiment, Landsat 8 has fewer observations than Sentinel-2, so individual inversions result in a very poor description of the dynamics of the parameter evolution over a year. It is also obvious that the single observations have large error bars, a consequence of the limited information content on each observation. The situation improves with Sentinel-2, as the number of observations increases. However, the dynamics are not well described by this experiment: the clustering of observations results in an incomplete retrieval of the temporal evolution of the different parameters. Once we start applying a dynamic model, we get interpolation, but also reduced uncertainties, with both Sentinel-2 and Landsat 8 being able to provide a reasonable path of the trajectory of the parameters. Once the dynamic model is established, it is straightforward to combine the observations from both sensors, resulting in a further reduced uncertainty.

2.2 Examples of synergistic use of IS and MS data

The theoretical discussion of potential synergies between optical IS and MS data presented in Section 2.1 is complemented in this section with a series of examples of how such synergies work for selected study cases including land use and land cover mapping, mineral exploration, vegetation parameter retrieval and water applications.

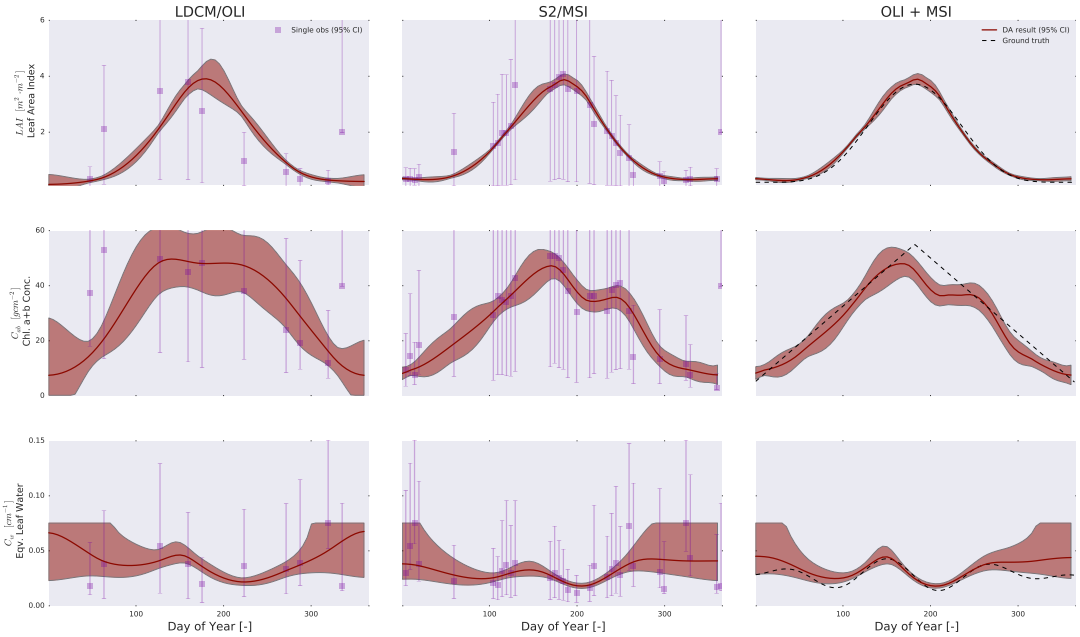

Fig. 5 Synthetic experiment demonstrating "data assimilation" system to invert land surface parameters from MS observations. Here, we have simulated a scene where leaf chlorophyll C_{ab}, leaf area index LAI and equivalent leaf water C_w vary over time. The retrieved LAI, C_{ab} and C_w are shown in each row (top to bottom, respectively). Each column shows the results of retrieving the parameters from Landsat 8 (left), Sentinel-2 MSI (center) and a combination of both. The dots with error bars refer to single observation inversions (mean and 1.96 times standard deviation), whereas the filled region shows the results of extending the inversions with a dynamic model and a variational data assimilation system.

2.2.1 Land use and land cover mapping

Land use and land cover (LULC) mapping is crucial to many scientific investigations from local to global scales. For decades, land cover maps are used for urban planning and a multitude of environmental monitoring applications such as urban expansion, forest inventory, biodiversity, land surface modeling, etc. LULC mapping with satellite data is one of the most widely investigated subjects.

In the last two decades, extensive efforts have been devoted to understand IS data for LULC mapping. However, airborne IS data are expensive and pose big processing challenges when coverage is very large, whereas the typical 30 m GSD of spaceborne IS missions is in general too coarse for many applications. To tackle this spatial issue, one possibility is to apply superresolution image reconstruction algorithms. Superresolution enhanced hyperspectral VNIR CHRIS/Proba data (9 m) data have been tested for land cover classification and unmixing (Chan et al., 2011). Demarchi et al. (2012) applied the same methodology for subpixel mapping. The impression is that these superresolution enhanced data sets have not been satisfactorily evaluated and hence their real potential remains uncertain. A major issue is the difficulty of compiling such data set with reliable groundtruth. Another issue is the algorithm evaluation method: how should the accuracy be evaluated for data sets acquired at different spatial resolution. Traditional accuracy measures for land cover classification have long been criticized as limited and problematic (Foody, 2002).

Recent development in pan-sharpening techniques and image fusion and the highly anticipated new spaceborne IS missions (e.g. EnMAP, HyspIRI) have ignited new momentum in the spatial enhancement of satellite IS images. While the issues related to an appropriate evaluation method still exist, one significant obstacle has been overcome – there will be real accessible data sets, such as EnMAP and Sentinel-2. Many

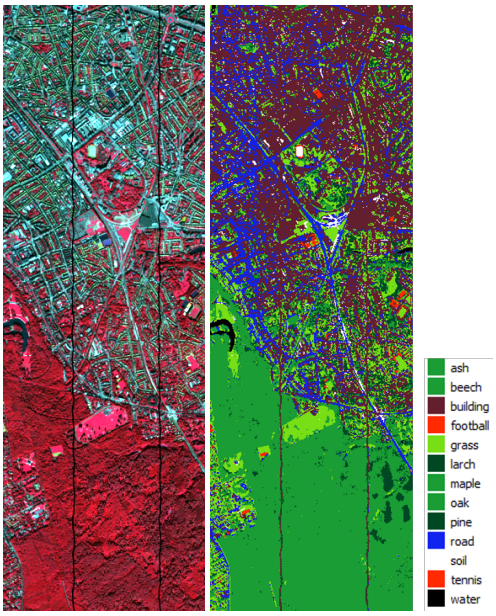

(a) (b)

Fig. 6 Land use and land cover mapping over Brussels. A false color composite of the study area from airborne APEX IS data is shown in (a), and a classification map using Canonical Correlation Forest (CCF) is depicted in (b).

methods fusing high resolution MS data and low-resolution IS data have been proposed targeting such future data sets. However, real examples of applying a fused and spatially-enhanced IS image for LULC classification are still comparatively rare.

To illustrate the usefulness of IS-MS fused images for LULC mapping, an APEX data set acquired from the Brussels capital region has been used. It has 288 bands between 400–2500 nm and is acquired at a GSD of 2.4 m (Chan and Yokoya, 2016). An EnMAP image with 242 bands is simulated with the EnMAP end-to-end simulator tool (Segl et al., 2012) at a 30 m GSD to mimic low-resolution IS data. A Sentinel-2 data set with 10 bands at 10 m and 20 m GSDs is also simulated using the S2eteS Sentinel-2 scene simulator (Segl et al., 2015). A generic 13-class land cover classification scheme is adapted for the study area: larch, pines, ash, maple, oak, beech, grassland (cropland, lawn and parks), buildings, roads, soil (bare soil, fallowed field, construction site), tennis court, football field, and water surface (artificial lake and canal). Fig. 6 shows the false color composite of the study area.

We compared the classification accuracy of EnMAP (30 m), Sentinel-2 (10 m and 20 m) and fused IS image at 10 m. The fusion approach has been described in Section 2.1.1. A groundtruth IS image at 10 m with the same spectral configuration as EnMAP is also simulated. All datasets are upscaled at 10 m with the same number of rows and columns for comparison. A total of 1095 pixels are blind-tested for accuracy. Two advanced classification algorithms, Rotation Forest (RF) (Rodriguez et al., 2006) and Canonical Correlation Forest (CCF) (Rainforth and Wood, 2015), are investigated. Fig. 6b shows the classification map generated from an IS image at 10 m resolution which is used as the benchmark for comparison; a legend with only 8 colors is used for easy visualization. Table 2 shows the overall accuracy, average class accuracy and kappa values of the classification results. In general, CCF performs better than RF. The benchmark 10 m IS data has achieved 70-74% (RF-CCF) overall accuracy. With Sentinel-2, the overall accuracy is 66-72%. With EnMAP at 30 m, the O.A. is 61-67%. For the fused IS data set, accuracies are 68%-73%. The performance

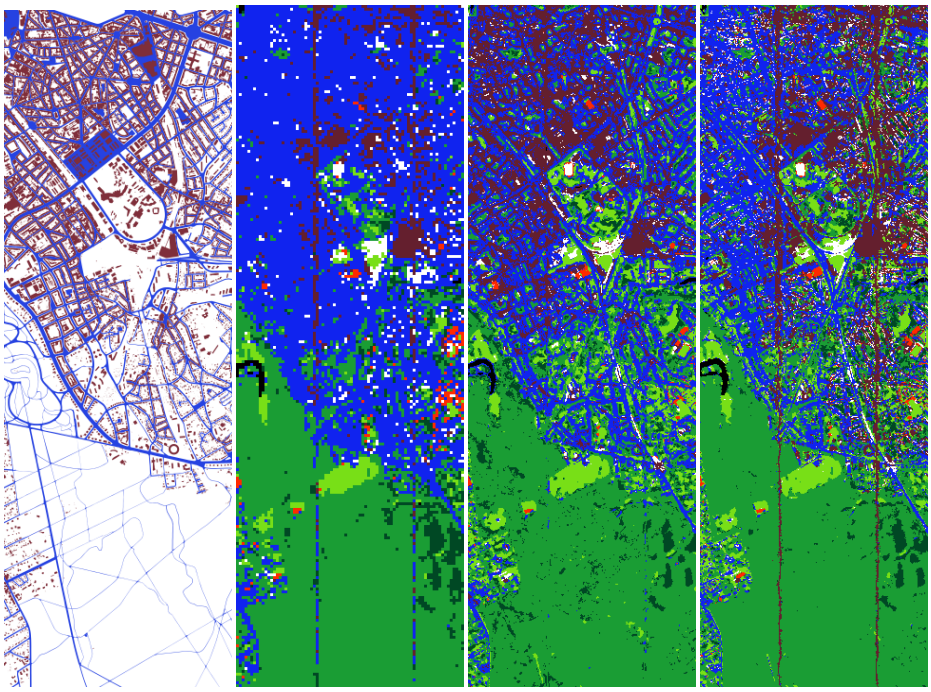

(a) (b) (c) (d)

Fig. 7 Ground-truth map of road and building classes (a) and classification results for EnMAP (b), Sentinel-2 (c) and fused image (d).

of the enhanced data is a little lower than the benchmark IS, moderately higher than the Sentinel-2, but significantly (5%) better than the 30 m EnMAP.

Fig. 7 clearly shows that the fused IS image reveals important details such as road networks comparable to Sentinel-2 but at a higher accuracy. Extraction and classification of urban objects such as road and buildings are understandably too challenging with EnMAP at 30 m resolution. This explains the high performance of Sentinel-2. Comparison between MS and IS for land cover classification have been widely studied and depending on the application; IS imagery does not always have superior performance (Xu and Gong, 2007). A MS-IS fusion approach is more suitable for challenging problems that require very rich spectral information and are better addressed with IS data. Our example shows that fusion of high-resolution MS and low-resolution IS images can achieve synergies in terms of significant improvement in classification details as compared with the low-resolution data and higher class accuracies as compared to the MS data. We expect the fusion synergies to have a significantly greater impact on specific LULC applications which require spatial details to characterize range, combination, distribution and clustering of species. For examples, urban mapping (Herold et al., 2004), vegetation species mapping (Chan and Paelinckx, 2008), and biodiversity information required for environmental assessments (Bush et al., 2017). Given the fact that spaceborne IS data at 30 m GSD will only be available in the next few years, the novelty of a potential fused IS data at high GSD (10 m) with large coverage is almost certain to attract new research momentum with innovative LULC applications.

Table 2 Comparison of classificacion accuracies with 13 classes. The highest accuracy is found for the reference data set, and the second highest for the fused data set. OA stands for overall accuracy and AA for average accuracy.

Classifier	**Rotation Forests**			**Canonical Correlation Forests**		
Accuracy	**OA**	**AA**	**Kappa**	**OA**	**AA**	**Kappa**
Reference	69.11	75.87	0.63	74.45	72.73	0.70
EnMAP	61.98	62.80	0.56	67.63	66.11	0.62
Sentinel-2	66.85	62.78	0.61	72.70	70.73	0.68
Fused	68.02	73.04	0.63	73.94	72.38	0.69

2.2.2 Mineral mapping

The Haib River Cu-Mo deposit in the lower Orange river region represents a unique test site for the demonstration of synergistic applications in geological remote sensing. Using simulations from HyMAP data, Mielke et al. (2014a) showed that it is possible to link data from state of the art MS systems such as Sentinel-2 and Landsat-8 to results from hyperspectral systems such as EnMAP via the IFD iron index introduced in Section 2.1.2. This absorption in the 900 nm region is caused by iron bearing minerals that may be produced by the weathering of metal sulfides such as pyrite and chalcopyrite (Chavez Jr., 2000). This process forms gossan surfaces that may be targeted with e.g. Sentinel-2, calculating the Normalized Iron Feature Depth from Sentinel-2 L1C data as shown in Fig. 8. The IFD is a simple three-point band depth index for MS sensor systems that proxies the band-depth of the iron feature near 900 nm using the two spectral bands which are closest to the shoulders of the 900 nm iron absorption feature (Mielke et al., 2014a). These two shoulder bands encompass the absorption band, which is closest to the 900 nm iron absorption feature (Mielke et al., 2014a). The feature depth is found by an interpolation of the aforementioned iron absorption feature band with the shoulder bands. The difference between interpolated and measured iron feature absorption band yields the IFD (Mielke et al., 2014b). This may be used in mineral exploration to highlight gossan zones that may indicate the presence of sulphide ore deposits (Taylor, 2011). If this concept is expanded to other sensors, for example ASTER SWIR measurements, it is possible to derive a false color composite of the normalized feature depths, which highlight the dominant material mixture at a specific location, shown for the Haib River area in Fig. 8b.

However, hyperspectral data from spaceborne sensors such as EnMAP or PRISMA are necessary for a more detailed mineral mapping using e.g. expert systems such as the EnMAP Geologic Mapper (EnGeoMAP) Base, which is a fully automated system for the detection of mineralogical surface cover types over mineral deposit areas (Mielke et al., 2016). IS may be used for a detailed view on the local dominant minerals in one area, as shown in Fig. 9. Here the gossan zones, which have been identified in Fig. 8 via the normalized iron feature depth may be subdivided into hematite, goethite and jarosite dominated gossans. Only IS data with its superior spectral resolution is able to correctly highlight and discriminate the most prominent minerals in the shortwave infrared from 2000 nm to 2500 nm. This shows the potential synergies in mineral exploration between large, multispectral, global mapping missions, such as Sentinel-2, and regional scale hyperspectral instruments such as EnMAP. The global mappers identify and highlight interesting anomalies for scientists working in mineral exploration, whilst IS data offers the capability to characterize these anomalies in much more detail using spectral geology tools such as EnGeoMAP for material identification.

2.2.3 Retrieval of vegetation parameters through model inversion

We can use the physical modeling introduced earlier to theoretically understand the limitations of different sensors for the retrieval of vegetation parameters, and how combining observations from different sensors might benefit parameter retrieval. To this end, we simulate a set of spectral acquisitions for EnMAP, as

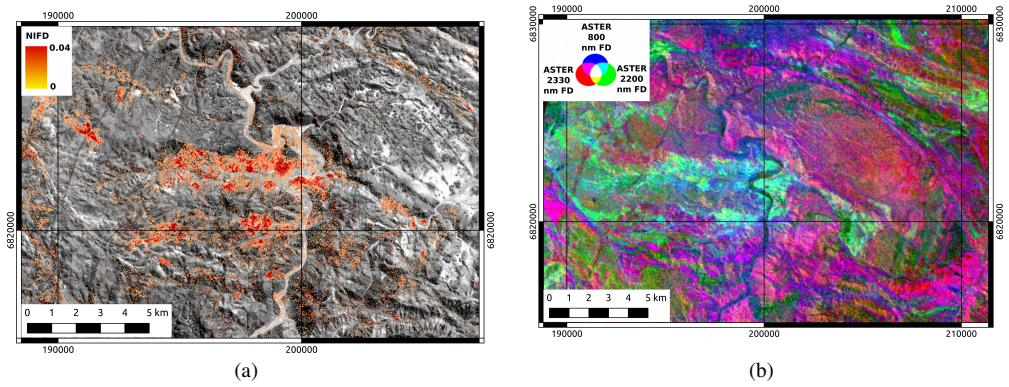

(a) (b)

Fig. 8 Indirect mapping of mineral types from multispectral remote sensing data over the Haib River Quartz Feldspar, Porphyrry. The Sentinel-2 normalized iron feature depth data, which highlights the main ore bearing unit, appears as a large oval shaped anomaly in the central part of the image in (a). ASTER normalized feature depth composite image is shown in (b). It highlights mineral mixtures that are dominated by absorption features near 2330 nm (red), e.g. epidote, chlorite and carbonates. Illite, alunite and muscovite dominated areas are colored in green. Areas with material that shows prominent iron absorption features are colored blue.

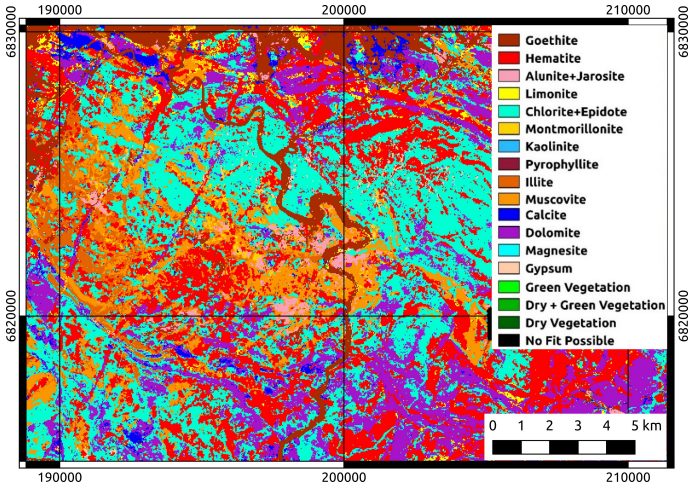

Fig. 9 EnGeoMAP Base classification result from simulated EnMAP data. The areas dominated by chlorite, epidote and carbonates correspond well to the areas colored in magenta and red in Fig. 8b.

well as simultaneous observations from Sentinel-2/MSI. The simulations are done using the PROSPECT-D leaf RT model (Féret et al., 2017) and the 4SAIL model (Verhoef, 1984) for leaf and canopy levels, respectively. The atmospheric effects are simulated by the 6S model (Vermote et al., 1997), taking into account the multiple interactions between land and atmosphere. The simulation thus presents a mapping from surface and atmospheric composition parameters to at-sensor reflectances. With some indication of the uncertainty in the observations at the sensor level, we can study the uncertainty of the retrieved parameters, under the assumption that the ”true state” of the combined surface and atmospheric system can be retrieved. This uncertainty is encoded in the posterior covariance matrix, which we approximate by a linearization of

the Hessian as in Lewis et al. (2012). We consider an scenario where we have a thick vegetation canopy (high LAI), and a moderate atmospheric loading. We can see the uncertainty associated with the retrieval of different parameters in the left hand side column of Fig. 10, which depicts the posterior correlation matrix, where a perfect retrieval would be indicated by an identity matrix. We can see that for a single EnMAP observation, a substantial number of off-diagonal elements are present, suggesting parameters that result in changes to the measured reflectance in the same spectral window cannot be individually differentiated with a single observation. This is unsurprising, and that is the reason that many retrieval schemes prescribe some of these parameters (e.g. the leaf structure parameter N, the parameter(s) controlling the leaf angle distribution, ALA, or prescribing a soil response). The left hand side of Fig. 10 is in essence a depiction of the ill-posedness of the inversion problem. It is important to note that this example is contrived, as no prior information has been used at all, which would not be the case on any practical scenario.

On the right hand side panel of Fig. 10, we show the posterior correlation matrix where the EnMAP observations have been optimally combined with the information retrieved from a Sentinel-2/MSI observation. We have assumed that these occur at different times, but close enough for the land surface to only have experienced a small change, but no extra information is gained on the atmospheric composition, and we have also ignored the 1375 nm band in Sentinel-2 MSI. It is clear that the posterior correlation matrices are much closer to a diagonal matrix, suggesting that some parameters such as leaf chlorophyll content, carotenoid content and anthocyanins might be well resolved. Other important parameters, such as LAI can be retrieved for high canopy cover, but the multiple scattering between the canopy and the atmosphere for low LAI results in a strong compensatory effect with aerosol optical thickness (AOT). Note that we cannot show the posterior covariance matrix for the Sentinel-2 MSI observation in this example: we are approximating the problem as a linear problem, in which we try to infer fourteen surface and atmosphere parameters, and with Sentinel-2 MSI we only have twelve bands, which results in an undetermined linear system.

Although in this example we have not assessed whether the solution can be found from the data, only what shape the uncertainty would take, the method used forms the basis of any Bayesian update, being the fundamental basis of techniques like Kalman or particle filters and smoothers (Gómez-Dans et al., 2016). Extended with a state vector dynamic model, the system would not only just provide inferences at the time of the acquisitions, but would also be able to optimally interpolate the state vector and provide uncertainty quantified inferences. The probabilistic basis of the Bayesian combination method rests on the two observations being interpreted by the same physical model with the same parameters, the assumption that the two sensors are accurately calibrated to a common standard, and that the different spatial resolutions can be bridged (by e.g. modeling the individual IFOV of the individual sensors). Provided these conditions are maintained, the method can be extended to other sensors.

2.2.4 Monitoring of inland and coastal waters

Regular observations of physical and biogeochemical components in inland and coastal waters provide essential information in the form of maps of water quality, bottom properties and bathymetry as needed for science and resource management (e.g. Palmer et al., 2015; Olmanson et al., 2008; Dekker et al., 2011; Mouw et al., 2015; Tyler et al., 2016). Depending on the scale of observations, the developments in water quality and biophysical parameter retrieval algorithms are driven by airborne IS (e.g. AVIRIS, APEX), ocean colour (OC) radiometry (e.g. MODIS, MERIS) and MS sensors (e.g. Landsat, Sentinel-2). In particular, the Sentinel-3/OLCI MS instrument offers an improve mapping potential for its specific capacities to resolve turbid, productive waters, and for having daily revisit with a 300 m GSD, whereas the Sentinel-2/MSI can provide data at a higher spatial resolution every 5 days. When combined with Landsat, a fine scale global mapping at a temporal resolution close to that of OC missions is also feasible. Finally, the previously mentioned IS satellite missions (e.g. EnMAP, PRISMA, HyspIRI) are anticipated to provide greatly enhanced capability to effectively enable wider applications for coastal and inland waters that, so far, have

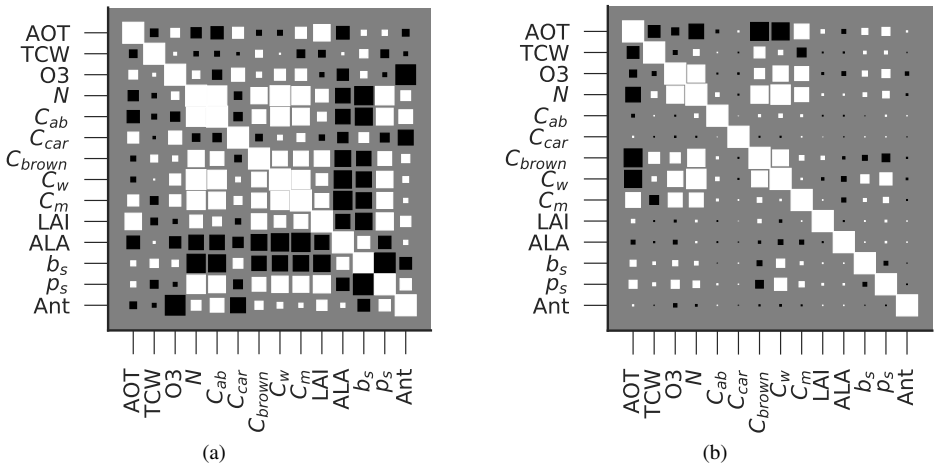

Fig. 10 Posterior correlation matrices for the combined land and atmosphere RT models PROSAIL and 6S used to invert a single observation from the EnMAP sensor (a), and the equivalent matrices when the EnMAP observation is supplemented with a contemporary Sentinel2/MSI observation (b). The variables in the axis correspond to 6S and PROSAIL input parameters. The white (... black) squares indicate positive (... negative) correlation, and the size of the square is proportional to its absolute value. Elements along the main diagonal have a correlation of one.

been mostly based on Hyperion (e.g. Kutser, 2004), HICO (e.g. Garcia et al., 2014) and CHRIS-Proba (e.g. Casal et al., 2011).

IS data in fact allows both to increase the estimation accuracy of inland and coastal water variables currently observed by OC and MS sensors and to access to new variables of interest (e.g. identification and quantification of particulate and dissolved matter: type and size of suspended particles, types of pigments, organic matter composition, cyanobacteria) for multiple applications (Hestir et al., 2015; Giardino et al., 2018). In such a context, a prime example regards phytoplankton, a key parameter for water managers and of considerable interest to scientists who are for instance interested to freshwater ecology. As a proxy of phytoplankton biomass, the chlorophyll-a concentration (chl-a), was mapped in lakes already in 1974 from aircraft and satellite (Strong, 1974). It also represents a primary parameter quantitatively derived from OC (Mishra et al., 2017). Then, IS provides further insights for detecting the accessory pigments of phytoplankton such as phycocyanin and phycoerythrin pigments, which are often associated to harmful algal blooms. As an example, in occasion of a red ciliate blooms in coastal waters, Dierssen et al. (2015) used OC MODIS to map the chl-a concentration and IS HICO to further distinguish phycoerythrin pigments. An additional application in which IS provided enhanced mapping capability occurs in shallow waters, (those where the bottom is visible from the water surface and measurably influences the remote sensing reflectance). The patchy structure typical of these environments hinder the use of OC sensors so that monitoring of bottom types and benthic communities (e.g. mud, sand-mud mixture, coral sands, coral reefs, seagrass, macrophytes) has been commonly achieved through MS sensors (e.g. Dekker et al., 2005). With a 10–30 m GSD, these sensors are ideal for most of the application scales, but are limited to identify species with similar spectral characteristics or to assess particular processes such as the state health of coral reefs (Botha et al., 2013). This is especially true for fine tracking of biodiversity and ecosystem functioning (identification of invasive and resident species). To this aim, airborne IS simultaneously providing high spatial and high spectral resolutions has been extensively used to make large-scale inventories of benthic photosynthetic organisms, such as macrophytes, seagrasses and corals (Phinn et al., 2008).

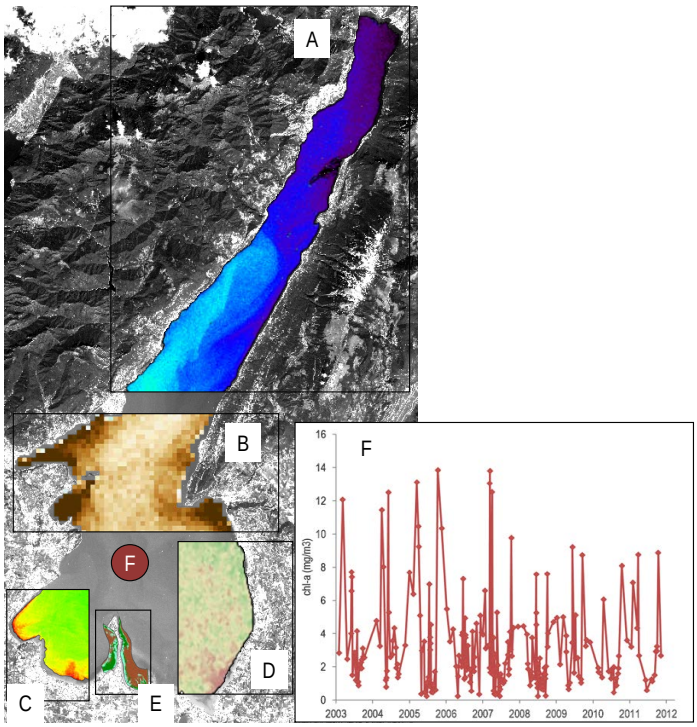

Fig. 11 An overview of satellite products developed for Lake Garda. A: total suspended matter (SPM) to trace water dynamics from Sentinel-2 (17-08-2016, from blue to green the SPM ranges from 0.1 to 2 g/m3); B: coloured dissolved organic matter (CDOM) as a results of primary producers degradation from MERIS (11-10-2006, from light- to dark-brown CDOM ranges from 0.01 to 0.1 m-1); C: fine scale mapping of chlorophyll-a concentrations from Sentinel-2 (17-08-2016, from green to red chl-a ranges from 2 to 5 mg/m3); D: map of cyanobacterial bloom from HICO (23-08-2012, from green-yellow-red the cyanobacterial index, as a proxy of its biomass, increases); E: substrate type from airborne IS data (15-07-2005, in brown nude substrates, from cyan to light-green to dark-green: submerged vegetation beds with increasing vegetation density cover); F: time-series of chl-a from a pelagic station from MERIS.

To summarise, the optical complexity of inland and coastal waters, which also usually show a fast degree of change and a patchy distribution of both water components and benthic habitats, make crucial synergic applications of IS and MS. Moreover, dealing with water optics, the availability of OC sensors has to be naturally included. As an example, we present the Lake Garda (Italy) test site, where at the beginning of the nineties, Zilioli et al. (1994) started to study the lake colour from Landsat. The lake is characterised by clear yet optically complex deep waters, with occasional cyanobacterial blooms and optically shallow areas with important submerged macrophyte beds, which make it challenging to develop robust retrieval algorithms. Nevertheless, the lake relevance (it is visited by more than 20 million tourists every year and stores about 50 km^3 of water, used both for recreational purposes and water supply) is demanding a series of applications that only synergistic use of IS, MS and OC are able to provide. Some of these applications (e.g. the support to the EU Water Framework Directive to report on both chl-a concentration and extension

of submerged vegetation beds) are qualitatively shown in Fig. 11. For the sake of brevity we can only mention that most of these applications (namely A, B, C and E) were developed based on Hyperion data, that was used as a bench-mark for establishing a sensor-independent physically-based approach (Giardino et al., 2007). The use of HICO was instead useful to recognise the spectral feature due to the phycocyanin (Fig. 11D) according to Kutser (2004), while the neural network C2R operationally provided the MERIS-derived chl-a time series (Fig. 11E). A complete description of the applications can be found in Bresciani et al. (2011, 2012).

3 Potential synergies of IS with non-optical remote sensing data

3.1 Synergies of IS with TIR data

TIR measurements hold a strong synergistic potential with optical data in general, and with IS in particular. The exploitation of synergies between VSWIR IS and multispectral TIR measurements is actually at the core of the NASA HyspIRI mission concept, which is intended to address a number of science questions focused on world ecosystems and natural hazards (Lee et al., 2015). HyspIRI is currently awaiting decision for implementation.

Based on the review by Lee et al. (2015), synergies between optical IS and multispectral TIR data can be important for, at least, the following applications:

- Canopy biochemistry: optical IS has demonstrated its potential to retrieve important leaf photosynthetic pigments, such as chlorophylls, carotenoids and anthocyanins, as well as leaf and canopy liquid water content (e.g. Ustin et al., 2004). This capability is well complemented by the ability of TIR measurements to measure other vegetation parameters such as cellulose, hemi-cellulose, cutin and other biochemicals with absorption features in the 8–14 μm region (Ribeiro da Luz and Crowley, 2007).
- Plant functioning: simultaneous measurements of vegetation biophysical and biochemical properties and surface temperature can help monitor plant physiological functioning and potential stress situations as well as to estimate evapotranspiration (Anderson and Kustas, 2008), which is important to e.g. agricultural applications, water use practices and mitigation strategies in response to drought.
- Earth surface composition and change: the composition of exposed rock and soils can benefit from synergies between optical IS and TIR measurements, as the combination of spectral reflectance and emissivity measurements has been shown to be very helpful in identifying rocks, minerals and soils (e.g. Calvin et al., 2015; Eisele et al., 2015) which is of especial important for geological applications of remote sensing (van der Meer et al., 2012). This is due to the fact that the spectral features of e.g. silicates, clay minerals, iron oxides and hydroxides from the VSWIR and TIR range complement each other perfectly to material discrimination and quantification.
- Wildfires: optical IS and TIR measurements yield complementary capabilities to understand wildfire processes, and in particular the coupling between fires, vegetation and associated trace gas emissions. TIR measurements can be used to calculate fire radiative power and temperature, whereas spectroscopic measurements in the SWIR can be used to distinguish small hotter fires from large cooler fires (Matheson and Dennison, 2012) as well as to evaluate fire severity and vegetation recovery (Veraverbeke et al., 2012).
- Volcanoes: in addition to the capabilities of TIR remote sensing to monitor changes in temperature and gases indicating volcanic activity, the combination with optical IS measurements can help predict lava flows through the characterization of effusion rate and temperature.
- Urban environments: although limited by the high spatial resolution ($<$5 m) typically required by urban applications, the combination of optical IS and TIR has been shown to be very useful to characterize urban environments. The IS provides a high power of discrimination of manmade materials through

the different spectral signatures, whereas TIR measurements can be used to measure temperatures and characterize the associated urban heat island effect (Roberts et al., 2012).

In addition to HyspIRI, concurrent IS and TIR measurements will also be available from the ISS through the coordinated operation of ECOSTRESS and HISUI (Stavros et al., 2017). Such combined measurements can be used for a preliminary assessment of some of HyspIRI's scientific questions.

3.2 Synergies of IS with LiDAR data

LiDAR is an active remote sensing technology, using the time of flight of a laser pulse to compute a distance between the instrument and the backscattering (reflecting) object. With a precise estimate of the location and orientation of the measurement platform, a 3d coordinate of the reflecting object can be computed. LiDAR can be applied across a range of scales, from ground-based instruments to space-borne designs, serving very different purposes, as e.g. surveying forest stands (Danson et al., 2007) or measuring the decline of the polar ice-caps (Zwally et al., 2002). The most common LiDAR implementation, however, is in airborne laser scanners (ALS), where LiDARs are combined with a scanner to cover an across flight-track swath. Very high scanning frequencies (modern systems send several hundred thousand laser pulses per second) provide detailed 3d point clouds of the earth's surface. This 3d data is of largest benefit for surface types that have inherent 3d features, e.g. urban areas and forests. For the latter, IS suffers from structural effects (Hilker et al., 2008) and consequently, the fusion of ALS and IS has the largest potential for forested areas. So far, most studies were focused on airborne instruments, as there were only few spaceborne IS instruments and LiDARs, and the latter only in very large footprints not well suited for vegetation studies (e.g. ICESAT GLAS). The fusion of IS and ALS can be performed at various levels of the processing chain, but accurate co-registration of the data sets is key to all approaches. One of the straightforward ways of synergistic use of IS and ALS is to use the ALS derived digital surface model (DSM) to geolocate the data of an IS system (typically push-broom sensors). Additional to the elevation model, more advanced approaches use both the IS and ALS intensity information in an overlapping wavelength domain (Fig. 12a) (Brell et al., 2016, 2017). This strategy enhances the synergistic use especially for the accurate co-registration of the two sensors (Brell et al., 2016).

In addition to the data level, fusion can as well be carried out at the product level, e.g. when combining two separate land-cover classifications based on separate IS and ALS data sets. Another aspect to classify fusion approaches is the choice of method. So far, most studies have used empirical frameworks for the fusion, e.g. a classifier or a regression model, but only few have used physical models of the radiative transfer to potentially improve results. A recent review of IS and ALS fusion approaches and their categorization by fusion level, approach and application can be found in Torabzadeh et al. (2014b). An important consideration is the notion of scale. IS and ALS data need to be similar in spatial extent and resolution for a genuine fusion of data sets. Larger mismatches in these two categories will result in methods being either up- or down-scaling or point-based cross-validation, e.g. in the case of a space-borne sampling LiDAR design (e.g. GEDI on the ISS) with a wall-to-wall IS instrument.

Empirical Approaches: Up to now, the majority of studies on IS and ALS fusion have used empirical approaches for land-cover classification (Torabzadeh et al., 2014b). In an early example, Koetz et al. (2008) fused IS and ALS data layers in a support vector machine framework to classify land-cover types including fuel-types in a wildland-urban interface to assess and mitigate forest fire risk. ALS and IS were highly complementary, having a much higher accuracy when combined, with the height information of ALS being particularly helpful for vegetation canopy height classes. Regarding tree species classification, accuracy for a temperate mixed forest comprising 8 species was increased from 75% when using either ALS or IS alone to 90% when combining the datasets (Torabzadeh et al., 2014a). Both ALS and IS features were aggregated

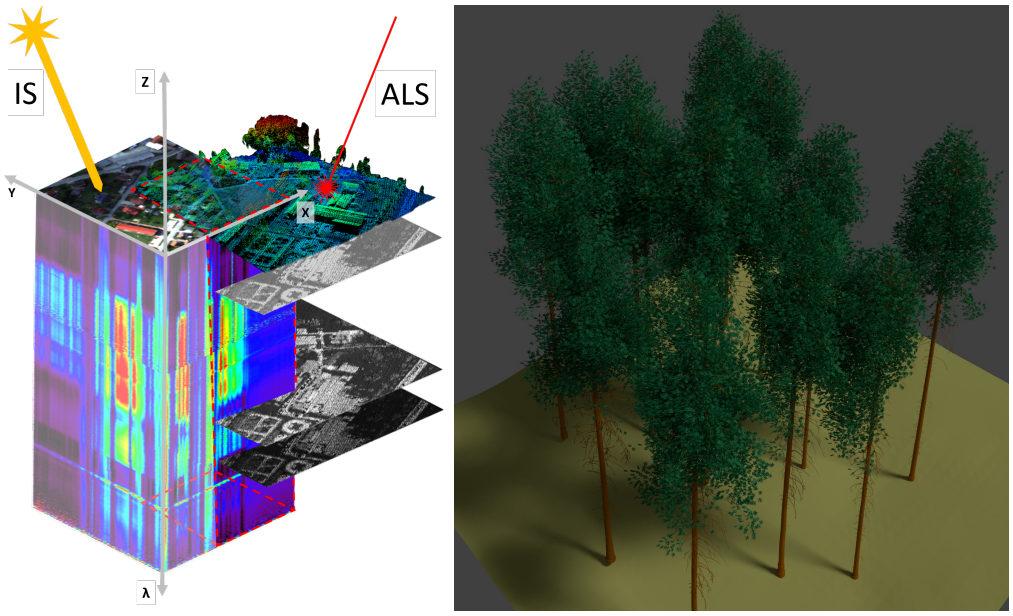

(a) (b)

Fig. 12 Combination of IS and LiDAR (airborne laser scanner, ALS) data. A schematic view of the combination is shown in (a), and a 3d model of a pine stand (Tharandt, Germany) reconstructed within the 3d vegetation laboratory project using laser scanning is displayed in (b). Laser scanning was at three different levels to model the pine stand: lab (for the shoot structure), ground (stems and branch structure) and airborne (tree locations and dimensions) (see Eysn et al. (2013) for details).

to individual tree crowns in this study. The high complementarity of ALS and IS for vegetation studies is as well confirmed by the large-scale campaigns and results of the Carnegie Airborne Observatory, flying IS and ALS sensors simultaneously, forming an ideal tool for 3d ecosystem assessment (Asner et al., 2012).

Physical Approaches: A potential tool to maximize the complementary exploitation of IS and ALS data are radiative transfer models, which add a physical layer in understanding and exploiting the signals recorded by both ALS and IS. A first of its kind, Koetz et al. (2007) used two different RTMs, one for IS, one for LiDAR, in a fused look-up table inversion retrieval of biochemical and biophysical variables such as LAI and fractional cover. However, results were mixed, likely hindered by the two models having distinct physical realities and differing parameterizations. For increased understanding of IS signals over vegetation, a possible solution is to derive an ALS based parameterization of the vegetation canopy, applied in an RTM to forward simulate the spectral response. This was successfully done with the ESA STSE “3d Vegetation Laboratory” - project (see Fig. 12b for an example 3d model) and such modeling tools will contribute to better fusion approaches for future missions (Schneider et al., 2017).

Besides the modeling approaches, physically based synergies between inflight IS and ALS data are being investigated. Based on radiative transfer modeling and ray-tracing approaches, the highly complementary sensor responses are physically adopted, and the active-passive dualism can be used to acquire more reliable and comparable hyperspectral data (Brell et al., 2017). This intensity based cross-calibration between the two sensors is a first physical based step to exploit active-passive synergies, with the specified goal of combining structural and spectral information for a comprehensive surface object description.

Level-0 fusion (multi-spectral LiDAR): The ultimate fusion of IS and ALS would be the development of a hyper-spectral LiDAR and implement that in an airborne design, remedying many issues of passive optical systems. However, up to now, only laboratory designs are truly hyperspectral due to their use a supercontinuum light source (Junttila et al., 2015), while the commercial ALS systems are multi-spectral only (3 wavelengths maximum in the Optech Titan system). In these implementations, however, not the small number of bands is the largest limitation, but the missing spatial and temporal synchronization of the wavelengths. This will lead to large errors for band ratios with only small signals (e.g. the photochemical reflectance index), as reflectance and structural differences are mixed between the different wavelengths. Only a design where all wavelengths sample exactly the same footprint (preferably at the same time) will provide accurate band ratios, which can be linked to foliage biochemistry (Morsdorf et al., 2009; Woodhouse et al., 2011).

Technology and system characteristic of spaceborne LiDAR instruments differ significantly from airborne systems. However, airborne based insights can be used for the development of synergies between various spectral and spatial sparse overlaps of spaceborne IS and LiDAR instruments. Upcoming systems like e.g. GEDI, ICESat-2 ATLAS (Abdalati et al., 2010) and the Methane Remote Sensing Lidar Mission (MERLIN) (Ehret et al., 2017) demonstrate the rapid advances in spaceborne LiDAR technology. This indicates that in the future, large footprints and the lack of spatial coverage will be overcome.

It must be stated that synergistic applications can also be found for the combination of IS with radar, although to a lesser extent than with LiDAR in part due to the non-overlapping wavelength domains. Demonstrated synergies between IS and radar are relatively similar to those between IS and LiDAR in the sense that radar provides the information on object structure to complete the spectral information from the IS image. Examples in the literature show the potential of synergies between IS and radar for the retrieval of vegetation properties (Treuhaft et al., 2002), urban mapping and land use classification (Hu et al., 2017) and oil spill mapping (Dabbiru et al., 2015).

4 Summary and conclusions

This contribution has discussed potential avenues for the synergistic use of IS and other sources of remote sensing data, with a focus on synergies with optical MS satellite missions because of their co-existence with spaceborne IS missions in the next years after the launch of EnMAP and PRISMA.

Optical IS and MS satellite missions can benefit from each other in two directions. On the one hand, IS acquisitions can be spatially-enhanced through fusion with higher spatial resolution MS data sets, as it would be the case of the combination of EnMAP and PRISMA with Sentinel-2 10–20 m GSD data. Such spatial sharpening of IS data has been shown to have a strong potential for LULC applications, and in especial for those dealing with urban environments. On the other hand, the spatio-temporal monitoring potential of wide-swath MS systems can be complemented by the rich spectral information in IS data. For example, IS data can be used to interprete and refine information retrieved from the MS data over a wider area through the addition of complementary information (e.g. for multi-sensor monitoring of the compositon of land surfaces and coastal and inland waters). The combination with IS data also allows to improve retrievals by MS systems through the extra spectral information provided by the IS data (e.g. endmembers derived from the IS data can be used as input for spectral unmixing techniques applied to the MS data). In the particular case of vegetation, for which relatively accurate physical radiative transfer models exist to link spectral reflectance with leaf and canopy parameters, model inversion and data assimilation techniques have a strong potential for parameter retrieval and the consistent merging of time series of MS and IS data.

Two other important aspects regarding optical IS and MS synergies have not been addressed in the text. First, the high spectral resolution and coverage of spaceborne IS instruments can be used to support calibration/validation activities of MS instruments in vicarious calibration exercises. Second, a wide range of optical MS missions with very high spatial resolution are being deployed by the private sector. These very

high spatial resolution data hold an even bigger potential for spatial enhacement of IS data than Sentinel-2. This is especially true for the Worldview-3 mission (DigitalGlobe Inc.) which includes several spectral channels in the SWIR which can be expected to substantially improve the fusion results with respect to Sentinel-2.

In addition to optical MS data, TIR data yield strong synergistic potential with optical IS data for a number of application domains including the monitoring of vegetation functioning, natural hazards and surface composition . Such a synergy of co-located IS-TIR observations is the basis of the HyspIRI mission concept currently under development by NASA (Lee et al., 2015). The potential of merging IS and LiDAR data for the characterization of e.g. vegetation covers and urban objects has been proven by several studies based on airborne data. Synergies of IS with both TIR and LiDAR data can be further tested through the joint operation of the HISUI spectrometer, the GEDI LiDAR and the ECOSTRESS multispectral TIR instrument to co-exist onboard the ISS (Stavros et al., 2017). However, the exploitation of such data set will be restricted to particular scientific studies because of the limited temporal and spatial overlap of the four instruments. In this regard, only the combination of optical IS and MS data can be considered for regular application in the next years thanks to the availability of Sentinel-2, Landsat and at least EnMAP and PRISMA in the 2018–2020 time frame. The development of unsupervised algorithms for the automatic co-location and synergistic exploitation of the two sources of data, either through the spatial enhancement of the IS data or the improvement of information extraction from the MS, can thus be considered as an important field of research in the next years. If such combined IS-MS data exploitation could become quasi-operational, it might have an impact on the definition of future spaceborne IS missions, as some observational requirements for the most demanding applications (e.g. spatial resolution for urban mapping) could be relaxed under the assumption that synergies with existing MS missions could compensate for such relaxation.

Acknowledgments

This paper is an outcome of a workshop on requirements, capabilities and directions in spaceborne imaging spectroscopy held at the International Space Science Institute (ISSI) in Bern, Switzerland, in November 2016. LG, KS, MB, and CM were partly funded by the EnMAP Scientific Preparation programme (FKZ:50EE1617).

References

Abdalati, W., Zwally, H. J., Bindschadler, R., Csatho, B., Farrell, S. L., Fricker, H. A., Harding, D., Kwok, R., Lefsky, M., Markus, T., Marshak, A., Neumann, T., Palm, S., Schutz, B., Smith, B., Spinhirne, J., and Webb, C. (2010). The icesat-2 laser altimetry mission. *Proceedings of the IEEE*, 98(5):735–751.

Anderson, M. and Kustas, W. (2008). Thermal remote sensing of drought and evapotranspiration. *Eos, Transactions American Geophysical Union*, 89(26):233–234.

Asner, G. P., Brodrick, P. G., Anderson, C. B., Vaughn, N., Knapp, D. E., and Martin, R. E. (2016). Progressive forest canopy water loss during the 2012–2015 california drought. *Proceedings of the National Academy of Sciences*, 113(2):E249–E255.

Asner, G. P., Knapp, D. E., Boardman, J., Green, R. O., Kennedy-Bowdoin, T., Eastwood, M., Martin, R. E., Anderson, C., and Field, C. B. (2012). Carnegie Airborne Observatory-2: Increasing science data dimensionality via high-fidelity multi-sensor fusion. *Remote Sensing of Environment*, 124(Supplement C):454 – 465.

Barnsley, M. J., Settle, J. J., Cutter, M., Lobb, D., and Teston, F. (2004). The PROBA/CHRIS mission: a low-cost smallsat for hyperspectral, multi-angle, observations of the Earth surface and atmosphere. *IEEE Transactions on Geoscience and Remote Sensing*, 42:1512–1520.

Bishop, C. A., Liu, J. G., and Mason, P. J. (2011). Hyperspectral remote sensing for mineral exploration in pulang, yunnan province, china. *International Journal of Remote Sensing*, 32(9):2409–2426.

Botha, E. J., Brando, V. E., Anstee, J. M., Dekker, A. G., and Sagar, S. (2013). Increased spectral resolution enhances coral detection under varying water conditions. *Remote Sensing of Environment*, 131(Supplement C):247 – 261.

Brell, M., Rogass, C., Segl, K., Bookhagen, B., and Guanter, L. (2016). Improving sensor fusion: A parametric method for the geometric coalignment of airborne hyperspectral and lidar data. *IEEE Transactions on Geoscience and Remote Sensing*, 54(6):3460–3474.

Brell, M., Segl, K., Guanter, L., and Bookhagen, B. (2017). Hyperspectral and lidar intensity data fusion: A framework for the rigorous correction of illumination, anisotropic effects, and cross calibration. *IEEE Transactions on Geoscience and Remote Sensing*, 55(5):2799–2810.

Bresciani, M., Bolpagni, R., Braga, F., Oggioni, A., and Giardino, C. (2012). Retrospective assessment of macrophytic communities in southern lake garda (italy) from in situ and mivis (multispectral infrared and visible imaging spectrometer) data. *Journal of Limnology*, 71(1):19.

Bresciani, M., Stroppiana, D., Odermatt, D., Morabito, G., and Giardino, C. (2011). Assessing remotely sensed chlorophyll-a for the implementation of the water framework directive in european perialpine lakes. *Science of The Total Environment*, 409(17):3083 – 3091.

Bush, A., Sollmann, R., Wilting, A., and et al. (2017). Connecting Earth Observation to High-Throughput Biodiversity Data. *NATURE ECOLOGY & EVOLUTION*, 1(0176).

Calvin, W. M., F. Littlefield, E., and Kratt, C. (2015). Remote sensing of geothermal-related minerals for resource exploration in nevada. 53:517–526.

Candela, L., Formaro, R., Guarini, R., Loizzo, R., Longo, F., and Varacalli, G. (2016). The prisma mission. In *2016 IEEE International Geoscience and Remote Sensing Symposium (IGARSS)*, pages 253–256.

Casal, G., Kutser, T., Domínguez-Gómez, J., Sánchez-Carnero, N., and Freire, J. (2011). Mapping benthic macroalgal communities in the coastal zone using chris-proba mode 2 images. *Estuarine, Coastal and Shelf Science*, 94(3):281 – 290.

Chan, J. C. W., Ma, J., de Voorde, T. V., and Canters, F. (2011). Preliminary results of superresolution-enhanced angular hyperspectral (chris/proba) images for land-cover classification. *IEEE Geoscience and Remote Sensing Letters*, 8(6):1011–1015.

Chan, J. C.-W. and Paelinckx, D. (2008). Evaluation of random forest and adaboost tree-based ensemble classification and spectral band selection for ecotope mapping using airborne hyperspectral imagery. *Remote Sensing of Environment*, 112(6):2999 – 3011.

Chan, J. C.-W. and Yokoya, N. (2016). Mapping land covers of brussels capital region using spatially enhanced hyperspectral images. In *WHISPERS 2016*, pages 1–5. IEEE Xplore.

Chavez Jr., W. (2000). Supergene oxidation of copper deposits: Zoning and distribution of copper oxide minerals. 41:9–21.

Chen, Z., Pu, H., Wang, B., and Jiang, G. M. (2014). Fusion of hyperspectral and multispectral images: A novel framework based on generalization of pan-sharpening methods. *IEEE Geoscience and Remote Sensing Letters*, 11(8):1418–1422.

Clark, R. N., Swayze, G. A., Livo, K. E., Kokaly, R. F., Sutley, S. J., Dalton, J. B., McDougal, R. R., and Gent, C. A. (2003). Imaging spectroscopy: Earth and planetary remote sensing with the usgs tetracorder and expert systems. *Journal of Geophysical Research: Planets*, 108(E12):n/a–n/a.

Dabbiru, L., Samiappan, S., Nobrega, R. A. A., Aanstoos, J. A., Younan, N. H., and Moorhead, R. J. (2015). Fusion of synthetic aperture radar and hyperspectral imagery to detect impacts of oil spill in gulf of mexico. In *2015 IEEE International Geoscience and Remote Sensing Symposium (IGARSS)*, pages 1901–1904.

753 Danson, F. M., Hetherington, D., Morsdorf, F., Koetz, B., and Allgower, B. (2007). Forest canopy gap
754 fraction from terrestrial laser scanning. *IEEE Geoscience and Remote Sensing Letters*, 4(1):157–160.
755 Dekker, A. G., Brando, V. E., and Anstee, J. M. (2005). Retrospective seagrass change detection in a
756 shallow coastal tidal australian lake. *Remote Sensing of Environment*, 97(4):415 – 433.
757 Dekker, A. G., Phinn, S. R., Anstee, J., Bissett, P., Brando, V. E., Casey, B., Fearns, P., Hedley, J.,
758 Klonowski, W., Lee, Z. P., Lynch, M., Lyons, M., Mobley, C., and Roelfsema, C. (2011). Intercom-
759 parison of shallow water bathymetry, hydro-optics, and benthos mapping techniques in australian and
760 caribbean coastal environments. *Limnology and Oceanography: Methods*, 9(9):396–425.
761 Demarchi, L., Chan, J. C.-W., Ma, J., and Canters, F. (2012). Mapping impervious surfaces from su-
762 perresolution enhanced chris/proba imagery using multiple endmember unmixing. *ISPRS Journal of*
763 *Photogrammetry and Remote Sensing*, 72(Supplement C):99 – 112.
764 Dierssen, H., Mcmanus, G., Chlus, A., Qiu, D., Gao, B.-C., and Lin, S. (2015). Space station image captures
765 a red tide ciliate bloom at high spectral and spatial resolution. 112.
766 Drusch, M., Bello, U. D., Carlier, S., Colin, O., Fernandez, V., Gascon, F., Hoersch, B., Isola, C., Laberinti,
767 P., Martimort, P., Meygret, A., Spoto, F., Sy, O., Marchese, F., and Bargellini, P. (2012). Sentinel-2:
768 Esa's optical high-resolution mission for {GMES} operational services. *Remote Sensing of Environment*,
769 120(0):25 – 36.
770 Drusch, M., Moreno, J., Bello, U. D., Franco, R., Goulas, Y., Huth, A., Kraft, S., Middleton, E. M., Migli-
771 etta, F., Mohammed, G., Nedbal, L., Rascher, U., Schüttemeyer, D., and Verhoef, W. (2017). The FLu-
772 orescence EXplorer Mission Concept – ESA's Earth Explorer 8. *IEEE Transactions on Geoscience and*
773 *Remote Sensing*, 55(3):1273–1284.
774 Ehret, G., Bousquet, P., Pierangelo, C., Alpers, M., Millet, B., Abshire, J. B., Bovensmann, H., Burrows,
775 J. P., Chevallier, F., Ciais, P., Crevoisier, C., Fix, A., Flamant, P., Frankenberg, C., Gibert, F., Heim,
776 B., Heimann, M., Houweling, S., Hubberten, H. W., Jöckel, P., Law, K., Löw, A., Marshall, J., Agusti-
777 Panareda, A., Payan, S., Prigent, C., Rairoux, P., Sachs, T., Scholze, M., and Wirth, M. (2017). Merlin:
778 A french-german space lidar mission dedicated to atmospheric methane. *Remote Sensing*, 9(10).
779 Eisele, A., Chabrillat, S., Hecker, C., Hewson, R., Lau, I. C., Rogass, C., Segl, K., Cudahy, T. J., Udelhoven,
780 T., Hostert, P., and Kaufmann, H. (2015). Advantages using the thermal infrared (tir) to detect and
781 quantify semi-arid soil properties. *Remote Sensing of Environment*, 163(Supplement C):296 – 311.
782 Eysn, L., Pfeifer, N., Ressl, C., Hollaus, M., Grafl, A., and Morsdorf, F. (2013). A practical approach for
783 extracting tree models in forest environments based on equirectangular projections of terrestrial laser
784 scans. *Remote Sensing*, 5(11):5424–5448.
785 Féret, J. B., Gitelson, A. A., Noble, S. D., and others (2017). PROSPECT-D: Towards modeling leaf optical
786 properties through a complete lifecycle. *Remote sensing of environment*.
787 Foody, G. M. (2002). Status of land cover classification accuracy assessment. *Remote Sensing of Environ-*
788 *ment*, 80(1):185 – 201.
789 Garcia, R. A., Fearns, P. R., and McKinna, L. I. (2014). Detecting trend and seasonal changes in bathymetry
790 derived from hico imagery: A case study of shark bay, western australia. *Remote Sensing of Environment*,
791 147(Supplement C):186 – 205.
792 Giardino, C., Brando, V. E., Dekker, A. G., Strömbeck, N., and Candiani, G. (2007). Assessment of water
793 quality in lake garda (italy) using hyperion. *Remote Sensing of Environment*, 109(2):183 – 195.
794 Giardino, C., Brando, V. E., Gege, P., Pinnel, N., Hochberg, E., Knaeps, E., Reusen, I., Doerffer, R., Bres-
795 ciani, M., Braga, F., Foerster, S., Champollion, N., and Dekker, A. (2018). Imaging spectrometry of
796 inland and coastal waters: State-of-the-art, achievements and perspectives. *Surveys in Geophysics*. in
797 press.
798 Goetz, A. F. H., Vane, G., Salomon, J. E., and Rock, B. N. (1985). Imaging spectroscopy for Earth remote
799 sensing. *Science*, 228:1147–1153.
800 Gómez-Dans, J., Lewis, P., and Disney, M. (2016). Efficient Emulation of Radiative Transfer Codes Using
801 Gaussian Processes and Application to Land Surface Parameter Inferences. *Remote Sensing*, 8(2):119.

Green, R. O., Eastwood, M., Sarture, C., Chrien, T., Aronsson, M., Chippendale, B., Faust, J., Pavri, B., Chovit, C., Solis, M., Olah, M., and Williams, O. (1998). Imaging spectroscopy and the airborne visible/infrared imaging spectrometer (AVIRIS). *Remote Sensing of Environment*, 65:227–248.

Grohnfeldt, C., Zhu, X. X., and Bamler, R. (2013). Jointly sparse fusion of hyperspectral and multispectral imagery. In *2013 IEEE International Geoscience and Remote Sensing Symposium - IGARSS*, pages 4090–4093.

Guanter, L., Kaufmann, H., Segl, K., Foerster, S., Rogass, C., Chabrillat, S., Kuester, T., Hollstein, A., Rossner, G., Chlebek, C., Straif, C., Fischer, S., Schrader, S., Storch, T., Heiden, U., Mueller, A., Bachmann, M., Mühle, H., Müller, R., Habermeyer, M., Ohndorf, A., Hill, J., Buddenbaum, H., Hostert, P., van der Linden, S., Leitão, P. J., Rabe, A., Doerffer, R., Krasemann, H., Xi, H., Mauser, W., Hank, T., Locherer, M., Rast, M., Staenz, K., and Sang, B. (2015). The enmap spaceborne imaging spectroscopy mission for earth observation. *Remote Sensing*, 7(7):8830–8857.

Herold, M., Roberts, D. A., Gardner, M. E., and Dennison, P. E. (2004). Spectrometry for urban area remote sensing—development and analysis of a spectral library from 350 to 2400 nm. *Remote Sensing of Environment*, 91(3):304 – 319.

Hestir, E. L., Brando, V. E., Bresciani, M., Giardino, C., Matta, E., Villa, P., and Dekker, A. G. (2015). Measuring freshwater aquatic ecosystems: The need for a hyperspectral global mapping satellite mission. *Remote Sensing of Environment*, 167(Supplement C):181 – 195. Special Issue on the Hyperspectral Infrared Imager (HyspIRI).

Hilker, T., Coops, N. C., Hall, F. G., Black, T. A., Wulder, M. A., Nesic, Z., and Krishnan, P. (2008). Separating physiologically and directionally induced changes in pri using brdf models. *Remote Sensing of Environment*, 112(6):2777 – 2788.

Hu, J., Mou, L., Schmitt, A., and Zhu, X. X. (2017). Fusionet: A two-stream convolutional neural network for urban scene classification using polsar and hyperspectral data. In *2017 Joint Urban Remote Sensing Event (JURSE)*, pages 1–4.

Hubbard, B. and Crowley, J. K. (2005). Mineral mapping on the chilean–bolivian altiplano using co-orbital ali, aster and hyperion imagery: Data dimensionality issues and solutions. 99:173–186.

Hubbard, B. E., Crowley, J. K., and Zimbelman, D. R. (2003). Comparative alteration mineral mapping using visible to shortwave infrared (0.4-2.4 mu;m) hyperion, ali, and aster imagery. *IEEE Transactions on Geoscience and Remote Sensing*, 41(6):1401–1410.

Junttila, S., Kaasalainen, S., Vastaranta, M., Hakala, T., Nevalainen, O., and Holopainen, M. (2015). Investigating bi-temporal hyperspectral lidar measurements from declined trees—experiences from laboratory test. *Remote Sensing*, 7(10):13863–13877.

Koetz, B., Morsdorf, F., van der Linden, S., Curt, T., and Allgöwer, B. (2008). Multi-source land cover classification for forest fire management based on imaging spectrometry and lidar data. *Forest Ecology and Management*, 256(3):263 – 271. Impacts of forest ecosystem management on greenhouse gas budgets.

Koetz, B., Sun, G., Morsdorf, F., Ranson, K., Kneubühler, M., Itten, K., and Allgöwer, B. (2007). Fusion of imaging spectrometer and lidar data over combined radiative transfer models for forest canopy characterization. *Remote Sensing of Environment*, 106(4):449 – 459.

Kutser, T. (2004). Quantitative detection of chlorophyll in cyanobacterial blooms by satellite remote sensing. *Limnology and Oceanography*, 49(6):2179–2189.

Lanaras, C., Baltsavias, E., and Schindler, K. (2015). Hyperspectral super-resolution by coupled spectral unmixing. In *The IEEE International Conference on Computer Vision (ICCV)*.

Lee, C. M., Cable, M. L., Hook, S. J., Green, R. O., Ustin, S. L., Mandl, D. J., and Middleton, E. M. (2015). An introduction to the nasa hyperspectral infrared imager (hyspiri) mission and preparatory activities. *Remote Sensing of Environment*, 167(Supplement C):6 – 19. Special Issue on the Hyperspectral Infrared Imager (HyspIRI).

Lewis, P., Gómez-Dans, J., Kaminski, T., Settle, J., Quaife, T., Gobron, N., Styles, J., and Berger, M. (2012). An Earth Observation Land Data Assimilation System (EO-LDAS). *Remote sensing of environment*,

120(0):219–235.

Lucke, R. L., Corson, M., McGlothlin, N. R., Butcher, S. D., Wood, D. L., Korwan, D. R., Li, R. R., Snyder, W. A., Davis, C. O., and Chen, D. T. (2011). Hyperspectral Imager for the Coastal Ocean: instrument description and first images. *Applied Optics*, 50(11):1501–1516.

Matheson, D. S. and Dennison, P. E. (2012). Evaluating the effects of spatial resolution on hyperspectral fire detection and temperature retrieval. *Remote Sensing of Environment*, 124(Supplement C):780 – 792.

Mielke, C., Boesche, N. K., Rogass, C., Kaufmann, H., Gauert, C., and de Wit, M. (2014a). Spaceborne Mine Waste Mineralogy Monitoring in South Africa, Applications for Modern Push-Broom Missions: Hyperion/OLI and EnMAP/Sentinel-2. *Remote Sensing*, 6(8):6790–6816.

Mielke, C., K. Boesche, N., Rogaß, C., Segl, K., Gauert, C., and Kaufmann, H. (2014b). Potential applications of the Sentinel-2 multispectral sensor and the EnMAP hyperspectral sensor in mineral exploration. In *EARSeL eProceedings*, volume 13, page 93.

Mielke, C., Rogass, C., Boesche, N., Segl, K., and Altenberger, U. (2016). EnGeoMAP 2.0 – Automated Hyperspectral Mineral Identification for the German EnMAP Space Mission. *Remote Sensing*, 8(2).

Milewski, R., Chabrillat, S., and Behling, R. (2017). Analyses of recent sediment surface dynamic of a namibian kalahari salt pan based on multitemporal landsat and hyperspectral hyperion data. *Remote Sensing*, 9(2).

Mishra, D., Ogashawara, I., and Gitelson, A. (2017). In *Bio-optical Modeling and Remote Sensing of Inland Waters*, page 332. Elsevier.

Morsdorf, F., Nichol, C., Malthus, T., and Woodhouse, I. H. (2009). Assessing forest structural and physiological information content of multi-spectral lidar waveforms by radiative transfer modelling. *Remote Sensing of Environment*, 113(10):2152 – 2163.

Mouw, C. B., Greb, S., Aurin, D., DiGiacomo, P. M., Lee, Z., Twardowski, M., Binding, C., Hu, C., Ma, R., Moore, T., Moses, W., and Craig, S. E. (2015). Aquatic color radiometry remote sensing of coastal and inland waters: Challenges and recommendations for future satellite missions. *Remote Sensing of Environment*, 160(Supplement C):15 – 30.

Olmanson, L. G., Bauer, M. E., and Brezonik, P. L. (2008). A 20-year landsat water clarity census of minnesota's 10,000 lakes. *Remote Sensing of Environment*, 112(11):4086 – 4097. Applications of Remote Sensing to Monitoring Freshwater and Estuarine Systems.

Palmer, S. C., Kutser, T., and Hunter, P. D. (2015). Remote sensing of inland waters: Challenges, progress and future directions. *Remote Sensing of Environment*, 157(Supplement C):1 – 8. Special Issue: Remote Sensing of Inland Waters.

Palsson, F., Sveinsson, J. R., Ulfarsson, M. O., and Benediktsson, J. A. (2016). Quantitative quality evaluation of pansharpened imagery: Consistency versus synthesis. *IEEE Transactions on Geoscience and Remote Sensing*, 54(3):1247–1259.

Phinn, S., Roelfsema, C., Dekker, A., Brando, V., and Anstee, J. (2008). Mapping seagrass species, cover and biomass in shallow waters: An assessment of satellite multi-spectral and airborne hyper-spectral imaging systems in moreton bay (australia). *Remote Sensing of Environment*, 112(8):3413 – 3425. Earth Observations for Marine and Coastal Biodiversity and Ecosystems Special Issue.

Rainforth, T. and Wood, F. (2015). Canonical Correlation Forests. *ArXiv e-prints*.

Ribeiro da Luz, B. and Crowley, J. K. (2007). Spectral reflectance and emissivity features of broad leaf plants: Prospects for remote sensing in the thermal infrared (8.0–14.0 μm). *Remote Sensing of Environment*, 109(4):393 – 405.

Roberts, D. A., Quattrochi, D. A., Hulley, G. C., Hook, S. J., and Green, R. O. (2012). Synergies between vswir and tir data for the urban environment: An evaluation of the potential for the hyperspectral infrared imager (hyspiri) decadal survey mission. *Remote Sensing of Environment*, 117(Supplement C):83 – 101. Remote Sensing of Urban Environments.

Rodriguez, J. J., Kuncheva, L. I., and Alonso, C. J. (2006). Rotation forest: A new classifier ensemble method. *IEEE Transactions on Pattern Analysis and Machine Intelligence*, 28(10):1619–1630.

Roy, D., Wulder, M., Loveland, T., C.E., W., Allen, R., Anderson, M., Helder, D., Irons, J., Johnson, D., Kennedy, R., Scambos, T., Schaaf, C., Schott, J., Sheng, Y., Vermote, E., Belward, A., Bindschadler, R., Cohen, W., Gao, F., Hipple, J., Hostert, P., Huntington, J., Justice, C., Kilic, A., Kovalskyy, V., Lee, Z., Lymburner, L., Masek, J., McCorkel, J., Shuai, Y., Trezza, R., Vogelmann, J., Wynne, R., and Zhu, Z. (2014). Landsat-8: Science and product vision for terrestrial global change research. *Remote Sensing of Environment*, 145(0):154 – 172.

Schmid, T., Koch, M., and Gumuzzio, J. (2005). Multisensor approach to determine changes of wetland characteristics in semiarid environments (central spain). *IEEE Transactions on Geoscience and Remote Sensing*, 43(11):2516–2525.

Schneider, F. D., Morsdorf, F., Schmid, B., Petchey, O. L., Hueni, A., Schimel, D. S., and Schaepman, M. E. (2017). Mapping functional diversity from remotely sensed morphological and physiological forest traits. *Nature Communications*.

Segl, K., Guanter, L., Gascon, F., Kuester, T., Rogass, C., and Mielke, C. (2015). S2etes: An end-to-end modeling tool for the simulation of sentinel-2 image products. *IEEE Transactions on Geoscience and Remote Sensing*, 53(10):5560–5571.

Segl, K., Guanter, L., Rogass, C., Kuester, T., Roessner, S., Kaufmann, H., Sang, B., Mogulsky, V., and Hofer, S. (2012). Eetes - the enmap end-to-end simulation tool. *IEEE Journal of Selected Topics in Applied Earth Observations and Remote Sensing*, 5(2):522–530.

Selva, M., Aiazzi, B., Butera, F., Chiarantini, L., and Baronti, S. (2015). Hyper-sharpening: A first approach on sim-ga data. *IEEE Journal of Selected Topics in Applied Earth Observations and Remote Sensing*, 8(6):3008–3024.

Stavros, E. N., Schimel, D., Pavlick, R., Serbin, S., Swann, A., Duncanson, L., Fisher, J. B., Fassnacht, F., Ustin, S., Dubayah, R., Schweiger, A., and Wennberg, P. (2017). ISS observations offer insights into plant function. *Nature Ecology & Evolution*, 1(0194).

Strong, A. E. (1974). Remote sensing of algal blooms by aircraft and satellite in lake erie and utah lake. *Remote Sensing of Environment*, 3(2):99 – 107.

Taylor, R. (2011). In *Gossans and Leached Cappings – Field Assessment*, page 146. Springer, Berlin-Heidelberg.

Thompson, D. R., Boardman, J. W., Eastwood, M. L., and Green, R. O. (2017). A large airborne survey of earth’s visible-infrared spectral dimensionality. *Opt. Express*, 25(8):9186–9195.

Torabzadeh, H., Morsdorf, F., Leiterer, R., and Schaepman, M. (2014a). Fusing imaging spectrometry and airborne laser scanning data for tree species discrimination. In *Geoscience and Remote Sensing Symposium (IGARSS), 2014 IEEE International*, pages 1253–1256.

Torabzadeh, H., Morsdorf, F., and Schaepman, M. E. (2014b). Fusion of imaging spectroscopy and airborne laser scanning data for characterization of forest ecosystems – a review. *ISPRS Journal of Photogrammetry and Remote Sensing*, 97(Supplement C):25 – 35.

Treuhaft, R. N., Asner, G. P., Law, B. E., and Van Tuyl, S. (2002). Forest leaf area density profiles from the quantitative fusion of radar and hyperspectral data. *Journal of Geophysical Research: Atmospheres*, 107(D21):ACL 7–1–ACL 7–13. 4568.

Tyler, A. N., Hunter, P. D., Spyrakos, E., Groom, S., Constantinescu, A. M., and Kitchen, J. (2016). Developments in earth observation for the assessment and monitoring of inland, transitional, coastal and shelf-sea waters. *Science of The Total Environment*, 572(Supplement C):1307 – 1321.

Ungar, S. G., Pearlman, J. S., Mendenhall, J. A., and Reuter, D. (2003). Overview of the Earth Observing One (EO-1) mission. *IEEE Transactions on Geoscience and Remote Sensing*, 41:1149–1159.

Ustin, S. L., Roberts, D. A., Gamon, J. A., Asner, G. P., and Green, R. O. (2004). Using imaging spectroscopy to study ecosystem processes and properties. *BioScience*, 54(6):523–534.

van der Meer, F. D., van der Werff, H. M., van Ruitenbeek, F. J., Hecker, C. A., Bakker, W. H., Noomen, M. F., van der Meijde, M., Carranza, E. J. M., de Smeth, J. B., and Woldai, T. (2012). Multi- and hyperspectral geologic remote sensing: A review. *International Journal of Applied Earth Observation*

and Geoinformation, 14(1):112 – 128.

Veraverbeke, S., Hook, S., and Harris, S. (2012). Synergy of vswir (0.4–2.5 μm) and mtir (3.5–12.5 μm) data for post-fire assessments. *Remote Sensing of Environment*, 124(Supplement C):771 – 779.

Verhoef, W. (1984). Light scattering by leaf layers with application to canopy reflectance modeling: The SAIL model. *Remote sensing of environment*, 16(2):125–141.

Vermote, E. F., Tanre, D., Deuze, J.-L., Herman, M., and Morcette, J.-J. (1997). Second Simulation of the Satellite Signal in the Solar Spectrum, 6S: an overview. *IEEE transactions on geoscience and remote sensing: a publication of the IEEE Geoscience and Remote Sensing Society*, 35(3):675–686.

Wei, Q., Dobigeon, N., and Tourneret, J. Y. (2015). Bayesian fusion of multi-band images. *IEEE Journal of Selected Topics in Signal Processing*, 9(6):1117–1127.

Woodhouse, I. H., Nichol, C., Sinclair, P., Jack, J., Morsdorf, F., Malthus, T. J., and Patenaude, G. (2011). A multispectral canopy lidar demonstrator project. *IEEE Geoscience and Remote Sensing Letters*, 8(5):839–843.

Xu, B. and Gong, P. (2007). Land-use/land-cover classification with multispectral and hyperspectral eo-1 data. 73:955–965.

Yokoya, N., Chan, J. C.-W., and Segl, K. (2016). Potential of resolution-enhanced hyperspectral data for mineral mapping using simulated enmap and sentinel-2 images. *Remote Sensing*, 8(3).

Yokoya, N., Grohnfeldt, C., and Chanussot, J. (2017). Hyperspectral and multispectral data fusion: A comparative review of the recent literature. *IEEE Geoscience and Remote Sensing Magazine*, 5(2):29–56.

Yokoya, N., Yairi, T., and Iwasaki, A. (2012). Coupled nonnegative matrix factorization unmixing for hyperspectral and multispectral data fusion. *IEEE Transactions on Geoscience and Remote Sensing*, 50(2):528–537.

Zilioli, E., Brivio, P., and Gomarasca, M. (1994). A correlation between optical properties from satellite data and some indicators of eutrophication in lake garda (italy). *Science of The Total Environment*, 158(Supplement C):127 – 133.

Zwally, H., Schutz, B., Abdalati, W., Abshire, J., Bentley, C., Brenner, A., Bufton, J., Dezio, J., Hancock, D., Harding, D., Herring, T., Minster, B., Quinn, K., Palm, S., Spinhirne, J., and Thomas, R. (2002). Icesat's laser measurements of polar ice, atmosphere, ocean, and land. *Journal of Geodynamics*, 34(3):405 – 445.